

DRI Call No. \_\_\_\_\_

Copy No. \_\_\_\_\_ of \_\_\_\_\_ cys.

*Final Report*

## VALIDATED-DATA REPORT FOR THE TOWER PHASE OF THE ARPA/OWEX PROGRAM

By: H. GUTHART

*Prepared for:*

MASSACHUSETTS INSTITUTE OF TECHNOLOGY  
LINCOLN LABORATORY  
P.O. BOX 73  
LEXINGTON, MASSACHUSETTS 02173

CONTRACT F19628-70-C-0230



STANFORD RESEARCH INSTITUTE  
Menlo Park, California 94025 • U.S.A.

ESD RECORD COPY  
RETURN TO  
SCIENTIFIC & TECHNICAL INFORMATION DIVISION  
(DRI), Building 1435

AD0758208

Approved for public release; distribution unlimited.

*Final Report*

*November 1972*

## **VALIDATED-DATA REPORT FOR THE TOWER PHASE OF THE ARPA/OWEX PROGRAM**

*By:* H. GUTHART

*Prepared for:*

MASSACHUSETTS INSTITUTE OF TECHNOLOGY  
LINCOLN LABORATORY  
P.O. BOX 73  
LEXINGTON, MASSACHUSETTS 02173

Purchase Order No. B-314

Prime Contract No. F19628-70-C-0230

ARPA Order No. 600

SRI Project 2106

*Approved by:*

T. MORITA, *Director*  
*Electromagnetic Sciences Laboratory*

RAY L. LEADABRAND, *Executive Director*  
*Electronics and Radio Sciences Division*

*Copy No. ....* **12**

## ABSTRACT

Instrumentation has been designed, developed, and operated to measure the statistics of wave-height fluctuations as well as the spatial-attenuation factor of capillary waves. A microwave radiometer was provided to measure the thermal emissions of the ocean surface at 8.9 GHz. This report highlights some of the data collected during the latter part of August 1972 on the NUC oceanographic tower.

Accepted for the Air Force  
Joseph J. Whelan, USAF  
Acting Chief, Lincoln Laboratory Liaison Office

## CONTENTS

ABSTRACT . . . . .	ii
LIST OF ILLUSTRATIONS . . . . .	iv
LIST OF TABLES . . . . .	vii
ACKNOWLEDGMENTS . . . . .	viii
I      INTRODUCTION . . . . .	1
II     WAVE-STAFF ARRAY . . . . .	2
A.    Temporal-Data Analysis . . . . .	6
B.    Spatial-Data Analysis . . . . .	17
C.    Wave-Direction Finding . . . . .	36
III    CAPILLARY-WAVE-ATTENUATION SENSOR . . . . .	40
IV    MICROWAVE RADIOMETER . . . . .	44
V    CONCLUSIONS AND RECOMMENDATIONS . . . . .	58

## ILLUSTRATIONS

1	Transfer Function for Wave-Staff Electronics . . . . .	3
2	Measured PSD Function of Wave-Height Fluctuations on San Francisco Bay for Different Probe Geometries . . . . .	4
3	Wave-Staff Array . . . . .	5
4	Temporal PSD Function of Wave-Height Fluctuations . . . . .	7
5	Autocorrelation Coefficient of Wave-Height Fluctuations . . . . .	7
6	Cross-Correlation Coefficient of Wave-Height Fluctuations Between Probes 3 and 4 . . . . .	8
7	Phase of the Cross Spectrum of Wave-Height Fluctuations Between Probes 3 and 4 . . . . .	8
8	Temporal PSD Function of Wave-Height Fluctuations on August 27 Beginning at 1012 . . . . .	9
9	Temporal PSD Function of Wave-Height Fluctuations on August 28 Beginning at 1001 . . . . .	10
10	Temporal PSD Function of Wave-Height Fluctuations on August 23 Beginning at 1319 . . . . .	11
11	Temporal Dependence of Wave Height at Discrete Frequencies for August 27 at 0951 . . . . .	12
12	Temporal Dependence of Wave Height at Discrete Frequencies for August 27 at 1155. . . . .	13
13	Temporal Dependence of Wave Height at Discrete Frequencies for August 28 at 0925.25 . . . . .	14
14	Temporal Dependence of Wave Height at Discrete Frequencies for August 28 at 1345.14 . . . . .	15
15	Temporal Dependence of Wave Height at Discrete Frequencies for August 28 at 1530.1 . . . . .	16
16	Calculated Spatial PSD Function for August 28 at 1101 (2.5-Minute Average) . . . . .	19
17	Calculated Spatial PSD Function for August 28 at 1001 <sup>2</sup> 0 dB Corresponds to 65 cm <sup>2</sup> -cm (14.5 Minute Average). . . . .	20

18	Calculated Spatial PSD Function for August 28 at 1016 0 dB Corresponds to $72 \text{ cm}^{-2}$ (14.5 Minute Average) . . . . .	21
19	Calculated Spatial PSD Function for August 28 at 1031 0 dB Corresponds to $89 \text{ cm}^{-2}$ (14.5 Minute Average) . . . . .	22
20	Calculated Spatial PSD Function for August 28 at 1046 0 dB Corresponds to $88 \text{ cm}^{-2}$ (14.5 Minute Average) . . . . .	23
21	Calculated Spatial PSD Function for August 28 at 1101 0 dB Corresponds to $93 \text{ cm}^{-2}$ (14.5 Minute Average) . . . . .	24
22	Calculated Spatial PSD Function for August 28 at 1116 0 dB Corresponds to $93 \text{ cm}^{-2}$ (14.5 Minute Average) . . . . .	25
23	Calculated Spatial PSD Function for August 28 at 1131 0 dB Corresponds to $76 \text{ cm}^{-2}$ (14.5 Minute Average) . . . . .	26
24	Calculated Spatial PSD Function for August 28 at 1146 0 dB Corresponds to $69 \text{ cm}^{-2}$ (14.5 Minute Average) . . . . .	27
25	Calculated Spatial PSD Function for August 27 at 1300 0 dB Corresponds to $23 \text{ cm}^{-2}$ (14.5 Minute Average) . . . . .	28
26	Calculated Spatail PSD Function for August 27 at 1315 0 dB Corresponds to $46 \text{ cm}^{-2}$ (14.5 Minute Average) . . . . .	29
27	Calculated Spatial PSD Function for August 27 at 1330 0 dB Corresponds to $36 \text{ cm}^{-2}$ (14.5 Minute Average) . . . . .	30
28	Calculated Spatial PSD Function for August 27 at 1345 0 dB Corresponds to $35 \text{ cm}^{-2}$ (14.5 Minute Average) . . . . .	31
29	Calculated Spatial PSD Function for August 23 at 1319 0 dB Corresponds to $38 \text{ cm}^{-2}$ (14.5 Minute Average) . . . . .	32
30	Calculated Spatial PSD Function for August 23 at 1334 0 dB Corresponds to $48 \text{ cm}^{-2}$ (14.5 Minute Average) . . . . .	33

31	Calculated Spatial PSD Function for August 23 at 1349 0 dB Corresponds to $38 \text{ cm}^{-2}$ (14.5 Minute Average) . . . . .	34
32	Calculated Spatial PSD Function for August 23 at 1404 0 dB Corresponds to $40 \text{ cm}^{-2}$ (14.5 Minute Average) . . . . .	35
33	Direction-Finding Formalism . . . . .	37
34	Schematic of Capillary-Wave-Attenuation Sensor . . . . .	41
35	Measured Spatial-Attenuation Factor . . . . .	42
36	Temporal Dependence of Radiometer and Band-Limited Wave-Staff Outputs for August 27 Beginning at 0951.0 . . . .	45
37	Temporal Dependence of Radiometer and Band-Limited Wave-Staff Outputs for August 27 Beginning at 116.35 . . . .	46
38	Temporal Dependence of Radiometer and Band-Limited Wave-Staff Outputs for August 27 Beginning at 1257.75. . . .	47
39	Temporal Dependence of Radiometer and Band-Limited Wave-Staff Outputs for August 27 Beginning at 1422.74. . . .	48
40	Temporal Dependence of Radiometer and Band-Limited Wave-Staff Outputs for August 27 Beginning at 1531.7 . . . .	49
41	Temporal Dependence of Radiometer and Band-Limited Wave-Staff Outputs for August 28 Beginning at 0934.0 . . . .	50
42	Temporal Dependence of Radiometer and Band-Limited Wave-Staff Outputs for August 28 Beginning at 1059.11. . . .	51
43	Temporal Dependence of Radiometer and Band-Limited Wave-Staff Outputs for August 28 Beginning at 1328.89. . . .	52
44	Temporal Dependence of Radiometer and Band-Limited Wave-Staff Outputs for August 28 Beginning at 1459.6 . . . .	53
45	Temporal Dependence of Radiometer and Band-Limited Wave-Staff Outputs for August 30 Beginning at 1050 . . . . .	54
46	Temporal Dependence of Radiometer and Band-Limited Wave-Staff Outputs for August 31 Beginning at 1230 . . . . .	55
47	Averaged Cross Correlation Between Radiometer and Amplitude of 6-Hz Component . . . . .	56
48	Averaged Cross Correlation Between Radiometer and Amplitude of 12-Hz Component . . . . .	56

## TABLES

#### ACKNOWLEDGMENTS

It is a pleasure to acknowledge the support and assistance of the following personnel, without whom the program could not have been completed: C. Blahnik for mechanical design and construction; G. R. Hilbers and R. T. Bly for electronic assistance; R. H. Martin for general support and operational assistance; R. C. Honey and R. E. Myers for the design of the capillary sensor; and D. G. Douglas for data-processing assistance.

## I INTRODUCTION

In the tower phase of the ARPA/OWEX, Stanford Research Institute (SRI) fielded three experiments. These were the following:

- (1) A wave-staff array for measuring the wave-height statistics.
- (2) A capillary-wave-attenuation sensor.
- (3) A microwave radiometer (this sensor was contributed to the experiment by SRI at no cost to the sponsor).

This data report describes the highlights of the measurements for selected time intervals and represents a fraction of the data recorded at the tower.

## II WAVE-STAFF ARRAY

The wave-staff array was mounted off the southwest corner of the tower as shown in the experimental plan.

Resistance-type wave staffs were used to sense wave-height fluctuations. The wave staffs were 0.025-cm-diameter nichrome wire of 1.2 m length, with a resistance of 25 ohms/meter.

To accomodate the anticipated dynamic range requirements, the transfer function of the probe electronics was designed to "pre-whiten" the wave-height fluctuations in the band of interest ( $1 \text{ hz} \leq f \leq 26 \text{ Hz}$ ) before analog-recording the data. Figure 1 shows the measured amplitude transfer function of the probe electronics. The solid line of this figure is a guide for the reader in estimating the frequency dependence of this characteristic.

To test the effects of shadowing of one probe in the array on a second probe, experiments were conducted on San Francisco Bay for different orientations of the two probes. Figure 2 shows the measured temporal power-spectral-density (PSD) function of wave-height fluctuations for different orientations of a probe pair separated 0.75 cm. It can be seen that the measured spectra are indistinguishable. These measurements indicate that the 0.025-cm wires introduce no significant perturbations on a second wire in its shadow.

Twelve wave staffs were arrayed off the NUC tower in a delta formation as shown in Figure 3, where the apex of the array was pointed to within  $10^\circ$  of west. Forty-three hours of data were recorded in the period August 23 through August 31. The minimum spacing in the array

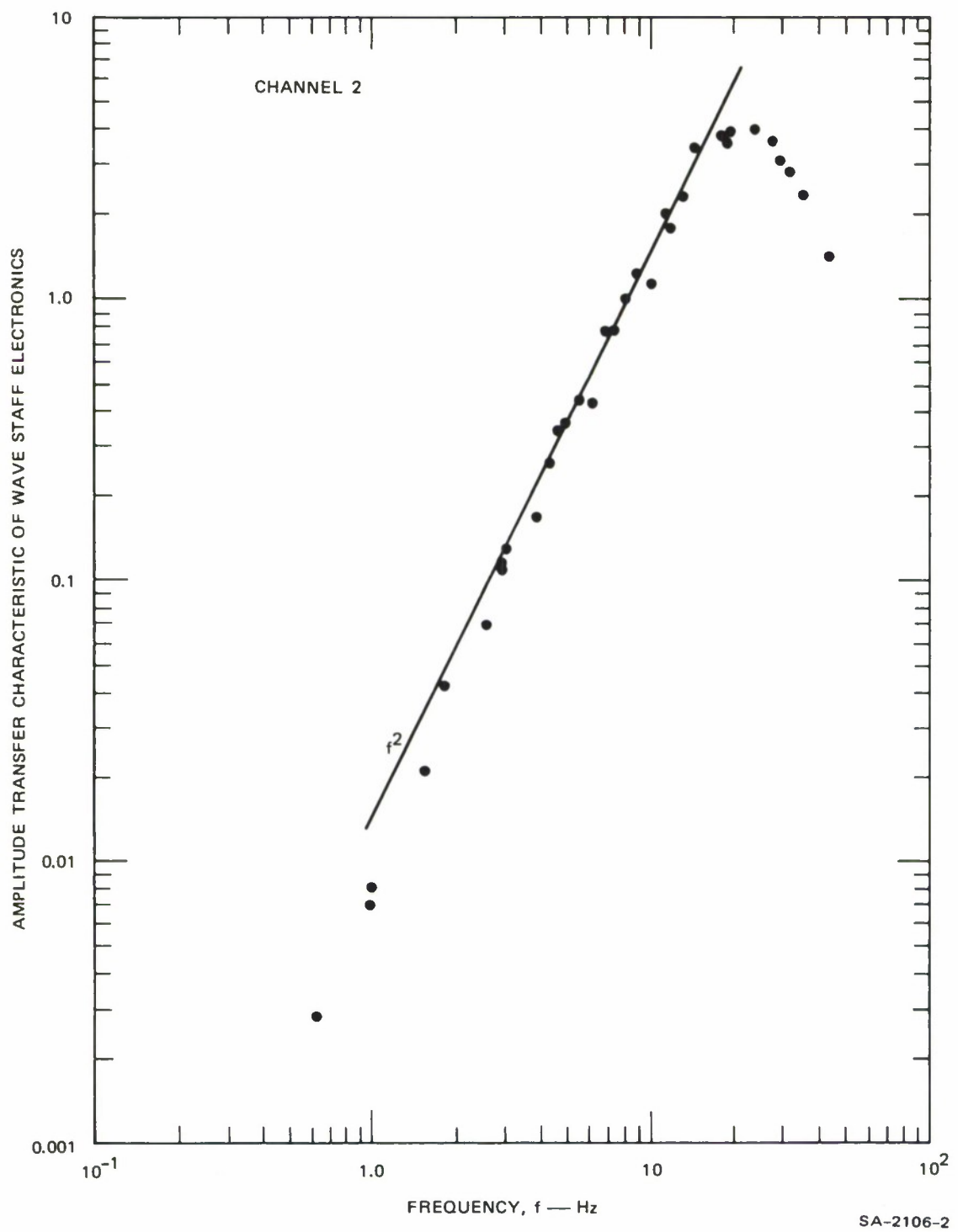


FIGURE 1 TRANSFER FUNCTION FOR WAVE-STAFF ELECTRONICS

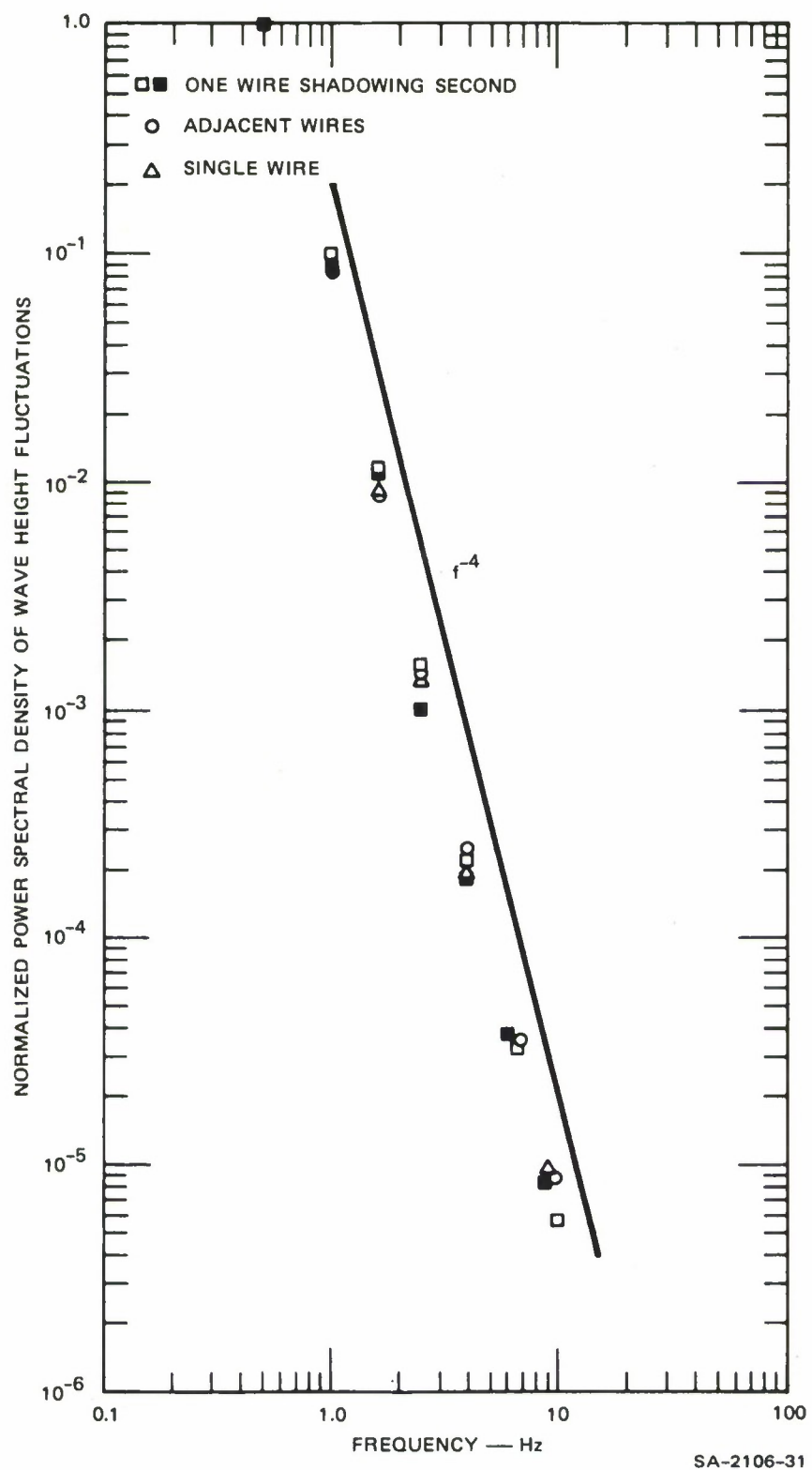


FIGURE 2 MEASURED PSD FUNCTION OF WAVE-HEIGHT FLUCTUATIONS ON SAN FRANCISCO BAY FOR DIFFERENT PROBE GEOMETRIES

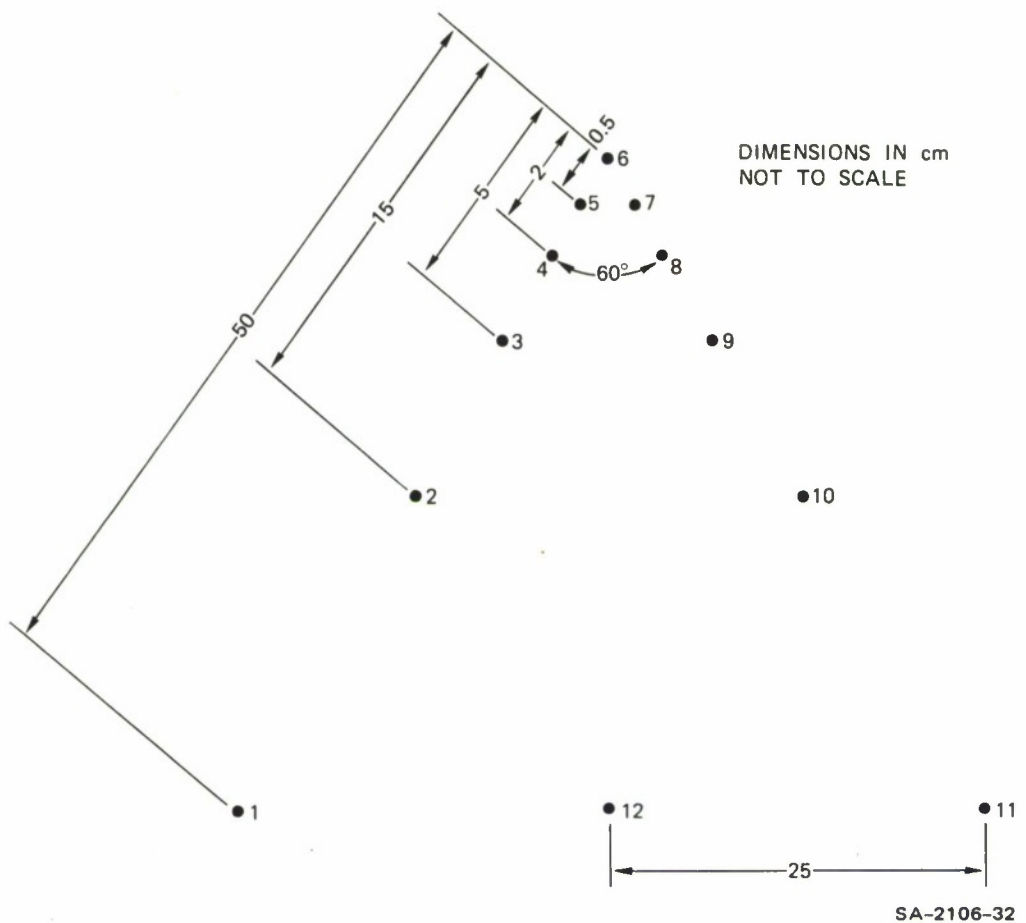


FIGURE 3 WAVE-STAFF ARRAY

was 0.5 cm (allowing resolution of waves of 1 cm wavelength), and the maximum spacing between probe pairs was 0.5 m. In the course of deploying the array, water seeped into the electronics package, destroying some of the cards and permitting the utilization of only eight probes (those numbered from 1 to 8 in Figure 3). The data from the probes were recorded on analog tape recorders.

The water surface was kept "nearly centered" on the wires of the array, in the face of 2-m swells, with a servo system driven by the low-frequency outputs of the wave staff.

The recorded wave-height data were shipped to SRI and digitized at a 58-Hz rate. This sampling frequency was chosen to exceed the frequency

corresponding to waves of 1 cm wavelength (as determined from the wave-dispersion relation). For each probe, the temporal PSD function and autocorrelation coefficient were computed with a 2.5-minute averaging time. Figures 4 and 5 show the format of the measured temporal PSD functions and the autocorrelation coefficient, respectively. The secondary peak in the spectrum at 5.5 Hz is always present in the data and was the subject of further analysis (to be discussed below). For every probe pair, the cross-correlation coefficient (a typical example of which is shown in Figure 6) and the phase of the cross spectrum (shown in Figure 7) was also computed. All of the foregoing were routinely processed for 2.5-minute averaging times, but there would be no difficulty in reprocessing the data for shorter averaging times.

#### A. Temporal-Data Analysis

Some representative temporal PSD functions for 3 hours of the total available data sample are shown in Figures 8 through 10. The spectra are shown at 15-minute intervals and have power-law dependencies for the several figures between -4.4 and -5 in the band between 1 and 25 Hz. It is observed that within an hour there are spectral fluctuations in which the high-frequency components have larger-percentage amplitude changes than the low-frequency components--i.e., the percentage modulation of the high-frequency waves exceeds that of the low-frequency waves.

As well as temporal spectra, the amplitude of discrete frequency components was monitored as a function of time (with 30-second averaging times) and is shown in Figures 11 through 15 for the 5-Hz, 10-Hz, 20-Hz, and 40-Hz components. In general, the activity at all frequencies correlates well, but the magnitude of the effect changes with frequency. Slicks are readily identified in these figures.

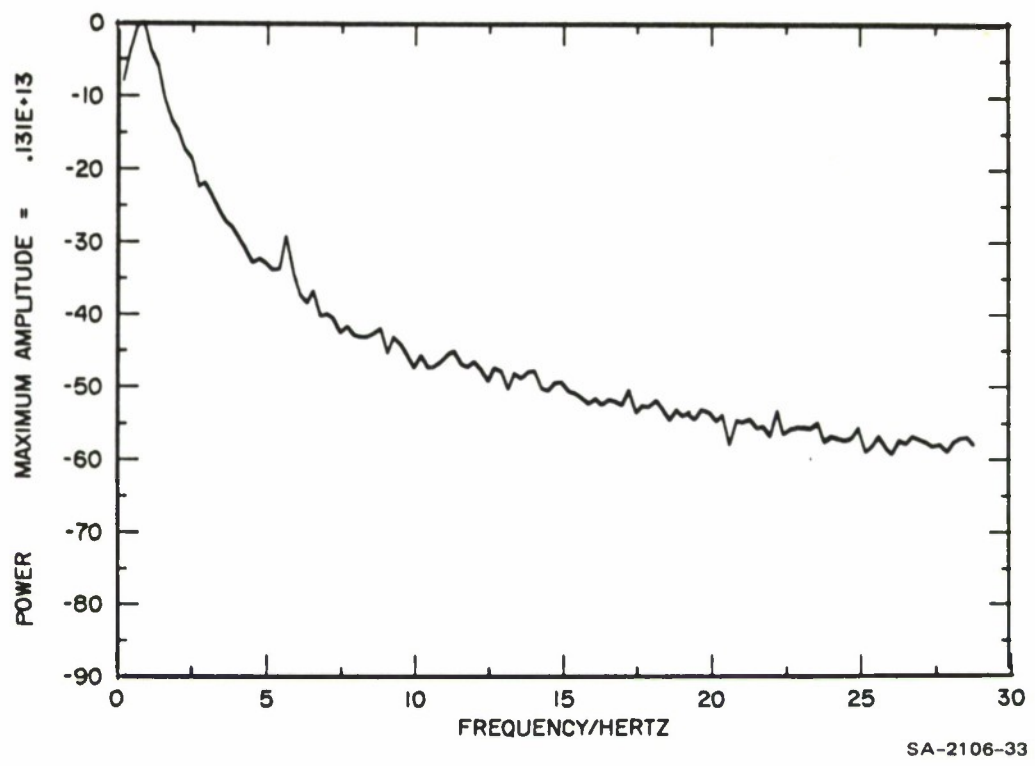


FIGURE 4 TEMPORAL PSD FUNCTION OF WAVE-HEIGHT FLUCTUATIONS

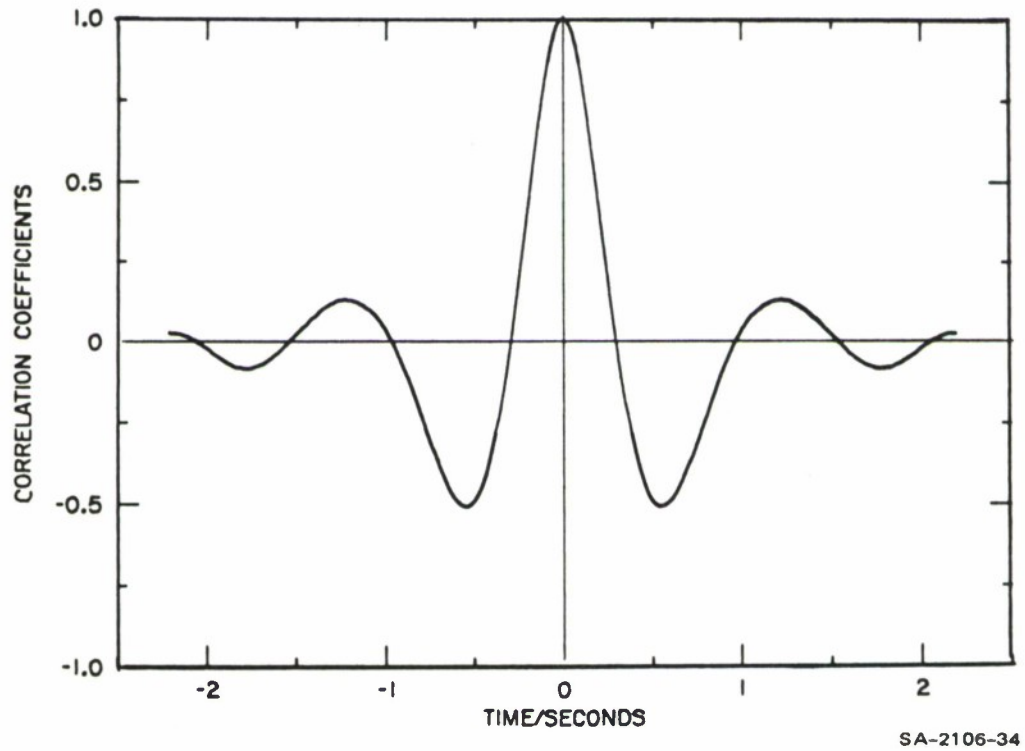
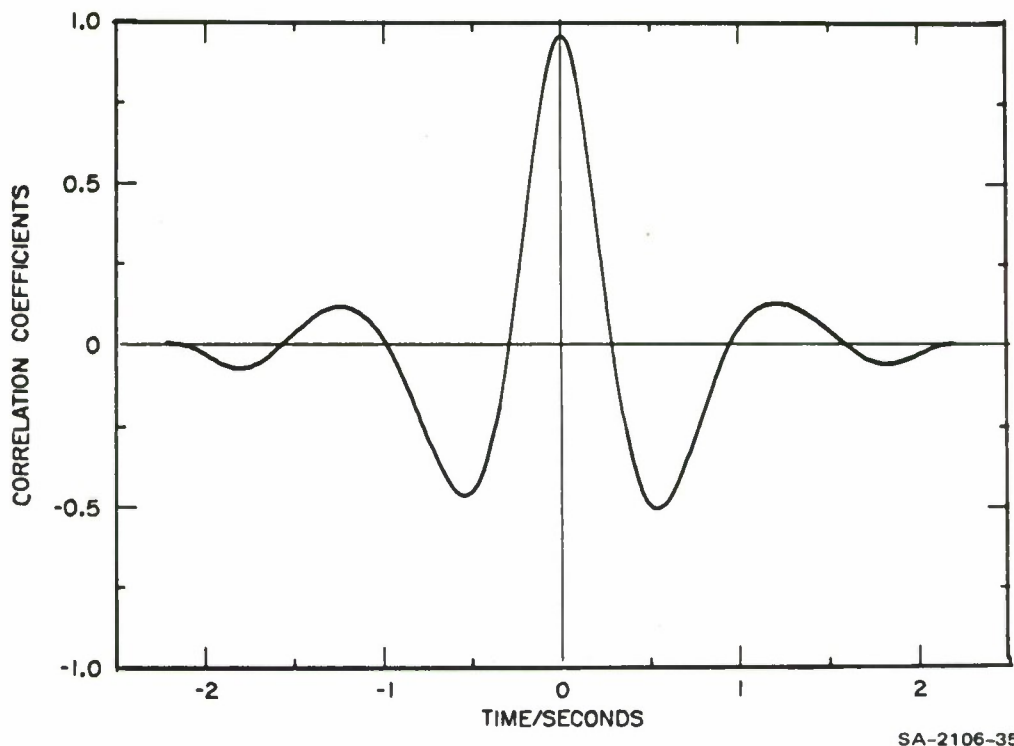
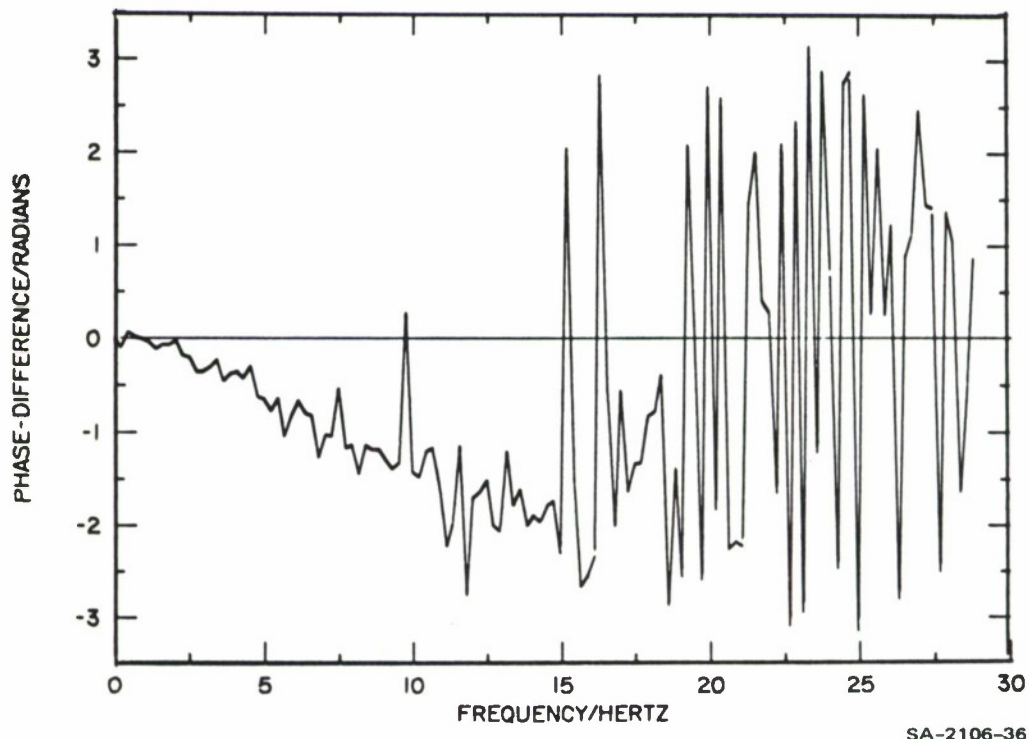


FIGURE 5 AUTOCORRELATION COEFFICIENT OF WAVE-HEIGHT FLUCTUATIONS



SA-2106-35

FIGURE 6 CROSS-CORRELATION COEFFICIENT OF WAVE-HEIGHT FLUCTUATIONS  
BETWEEN PROBES 3 AND 4



SA-2106-36

FIGURE 7 PHASE OF THE CROSS SPECTRUM OF WAVE-HEIGHT FLUCTUATION  
BETWEEN PROBES 3 AND 4

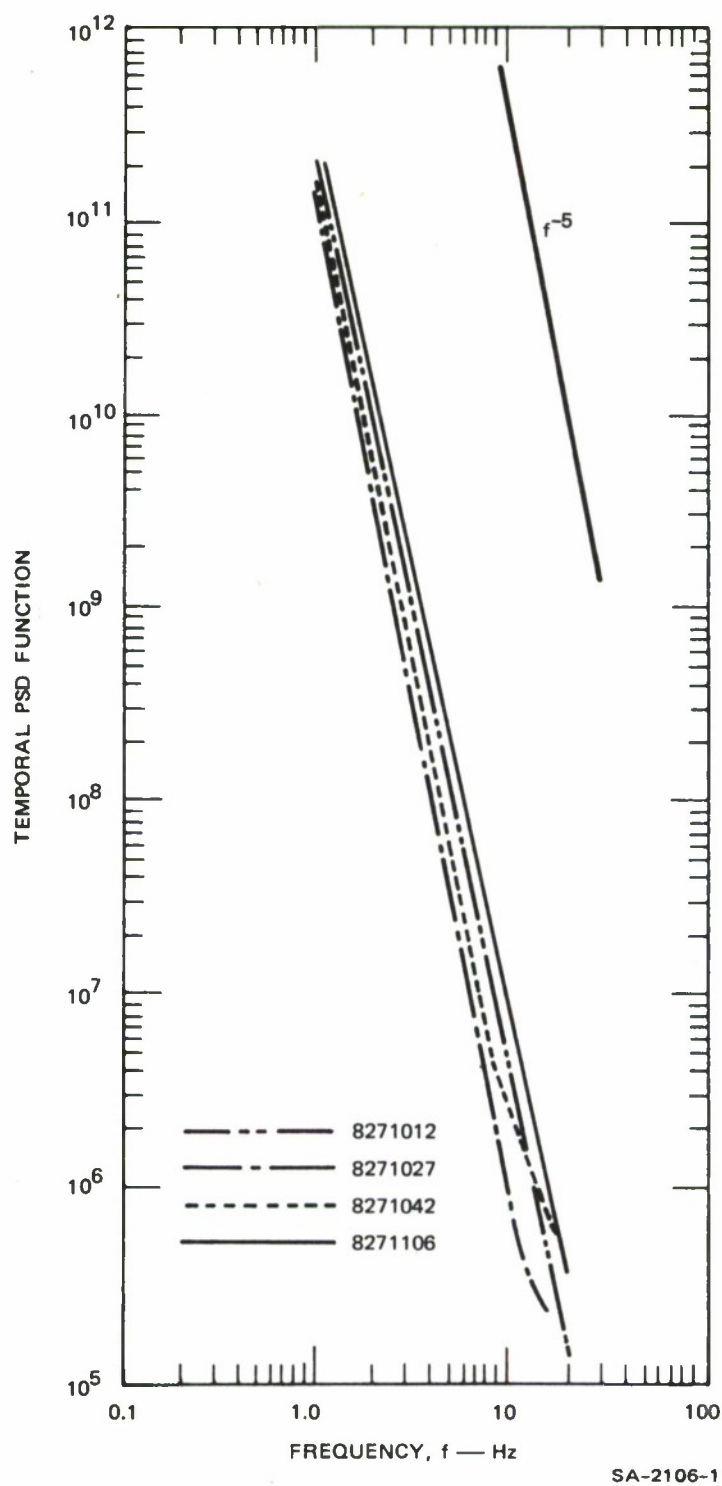


FIGURE 8 TEMPORAL PSD FUNCTION OF WAVE-HEIGHT FLUCTUATIONS ON AUGUST 27 BEGINNING AT 1012

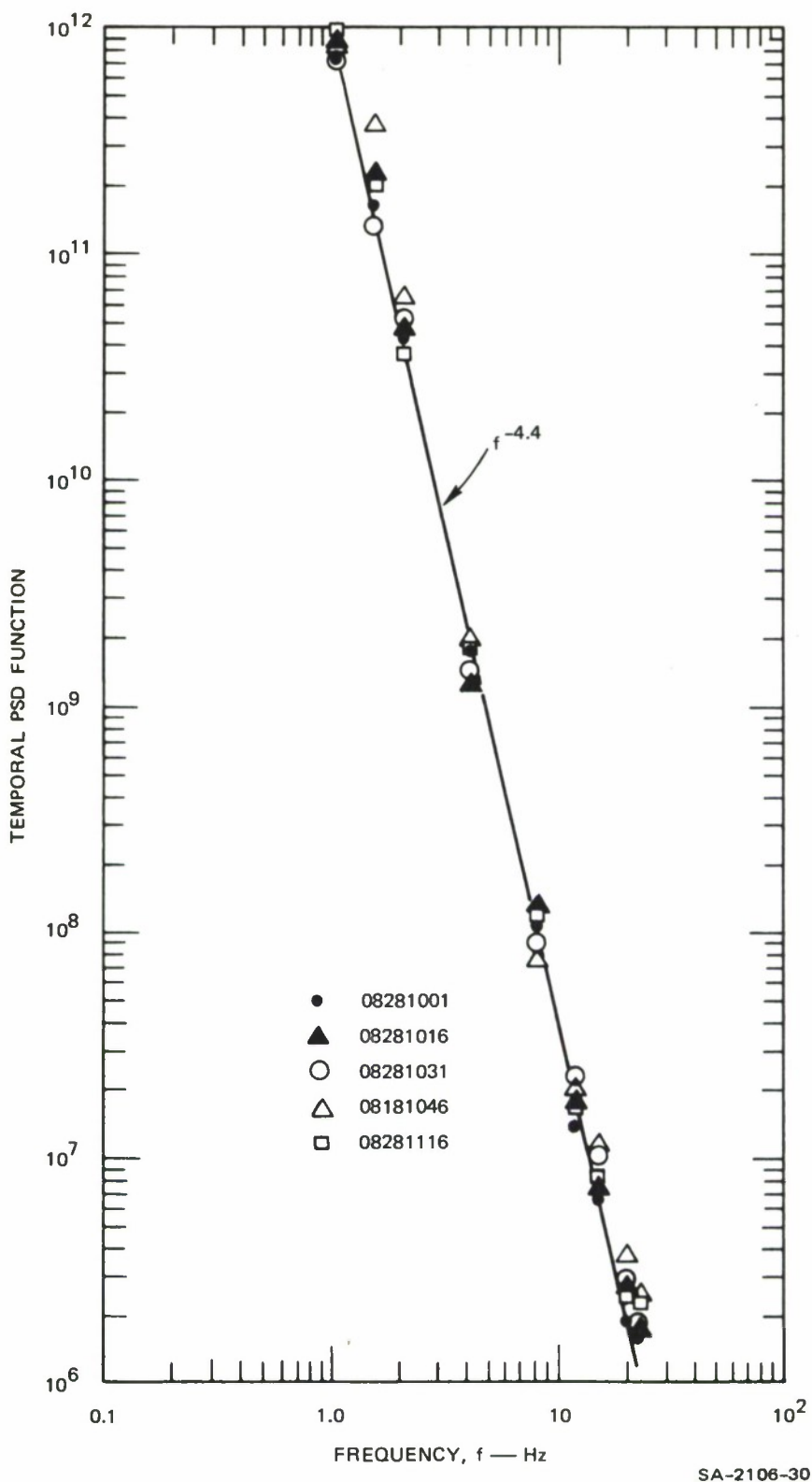


FIGURE 9 TEMPORAL PSD FUNCTION OF WAVE-HEIGHT FLUCTUATIONS ON AUGUST 28 BEGINNING AT 1001

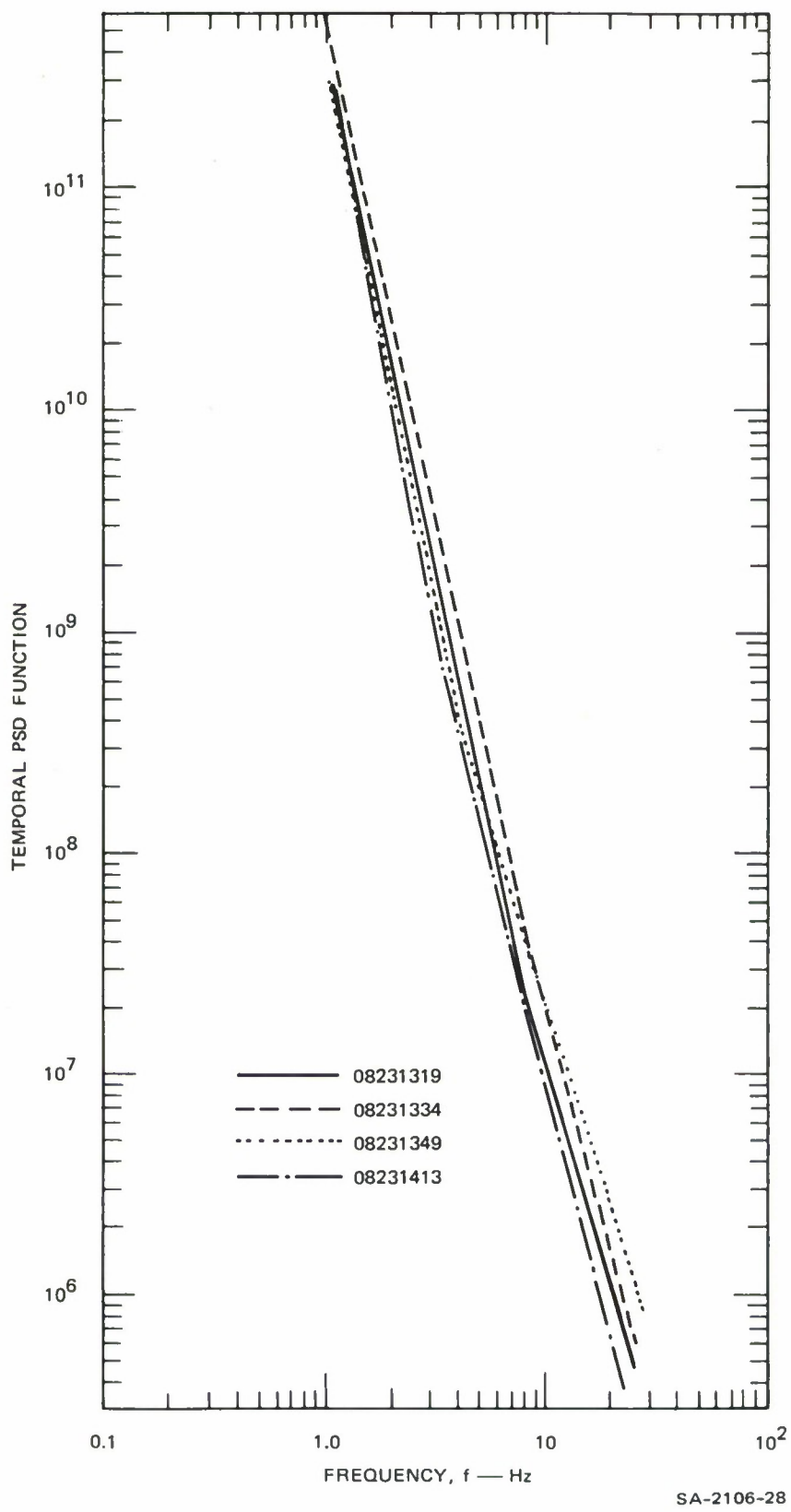


FIGURE 10 TEMPORAL PSD FUNCTION OF WAVE-HEIGHT FLUCTUATIONS ON AUGUST 23 BEGINNING AT 1319

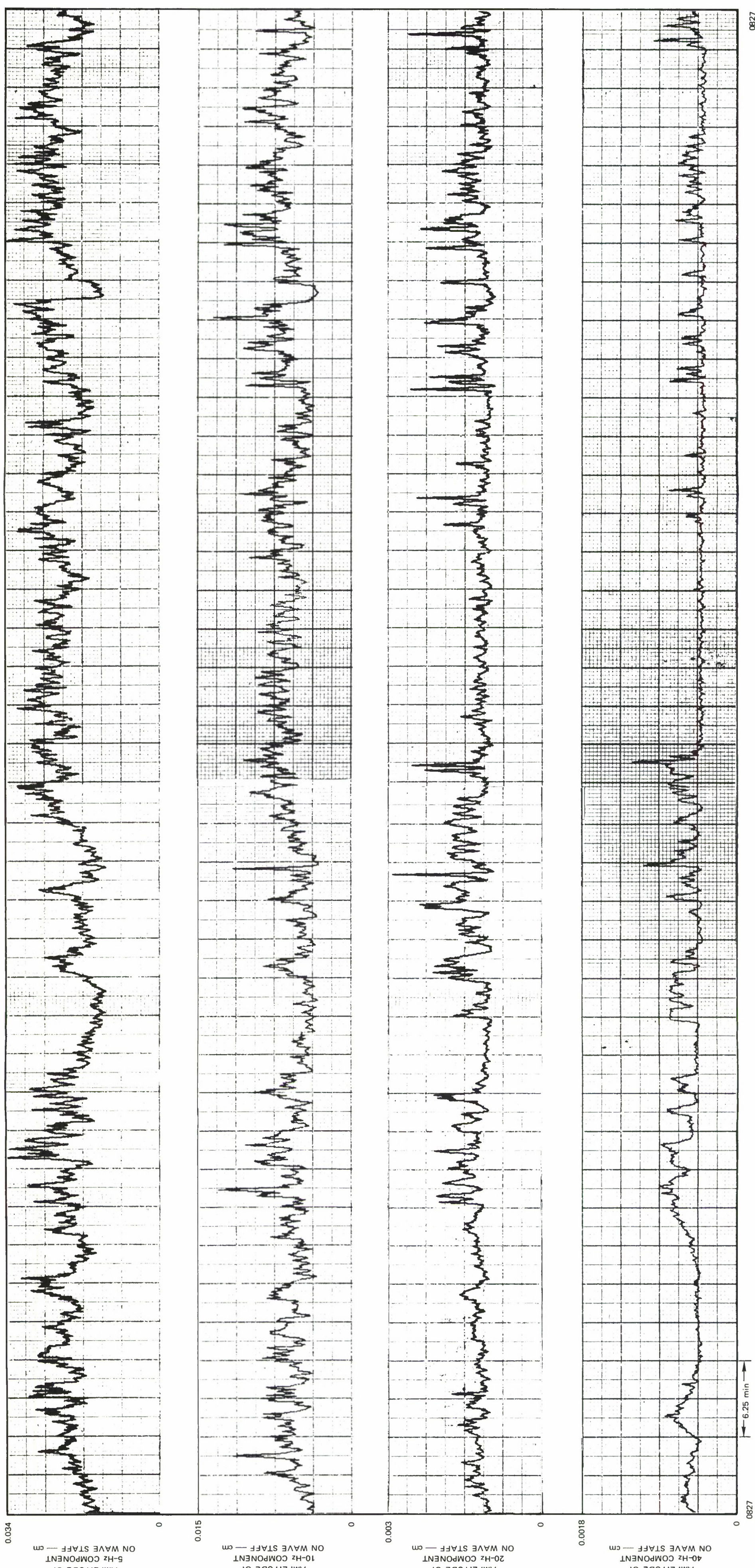


FIGURE 11 TEMPORAL DEPENDENCE OF WAVE HEIGHT AT DISCRETE FREQUENCIES FOR AUGUST 27 AT 0951

0827  
1152.5  
SA-2106-37

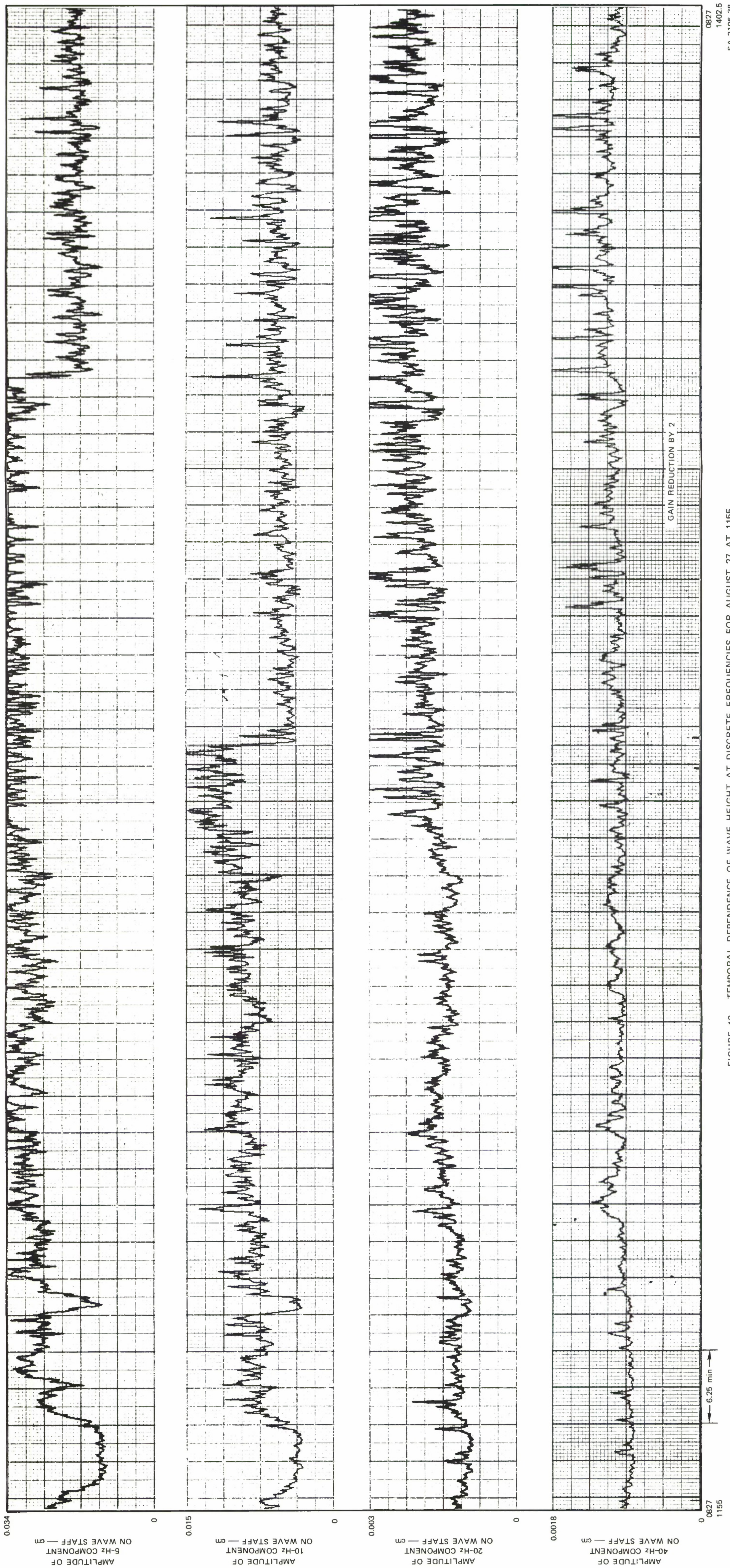
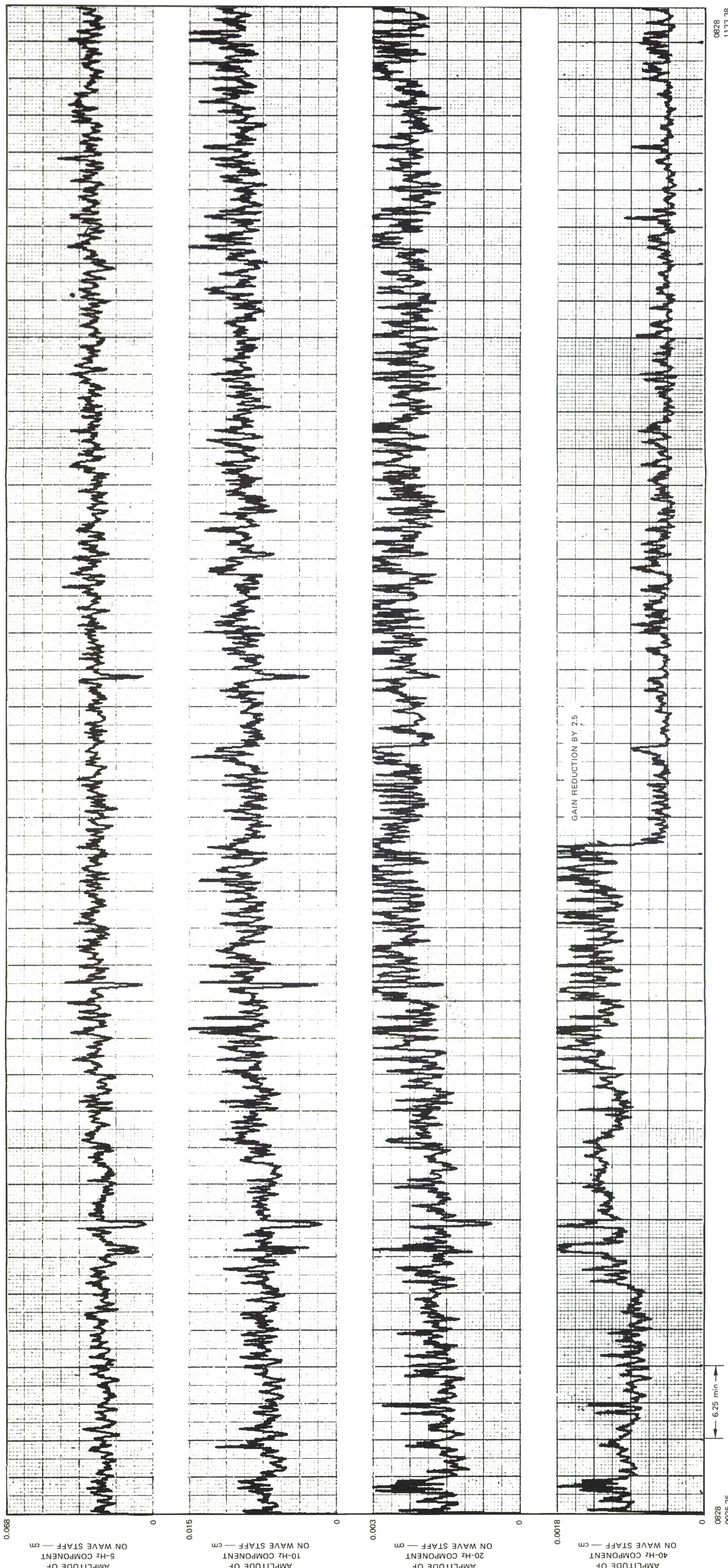


FIGURE 12 TEMPORAL DEPENDENCE OF WAVE HEIGHT AT DISCRETE FREQUENCIES FOR AUGUST 27 AT 1155

0827  
14025  
SA-2106-38



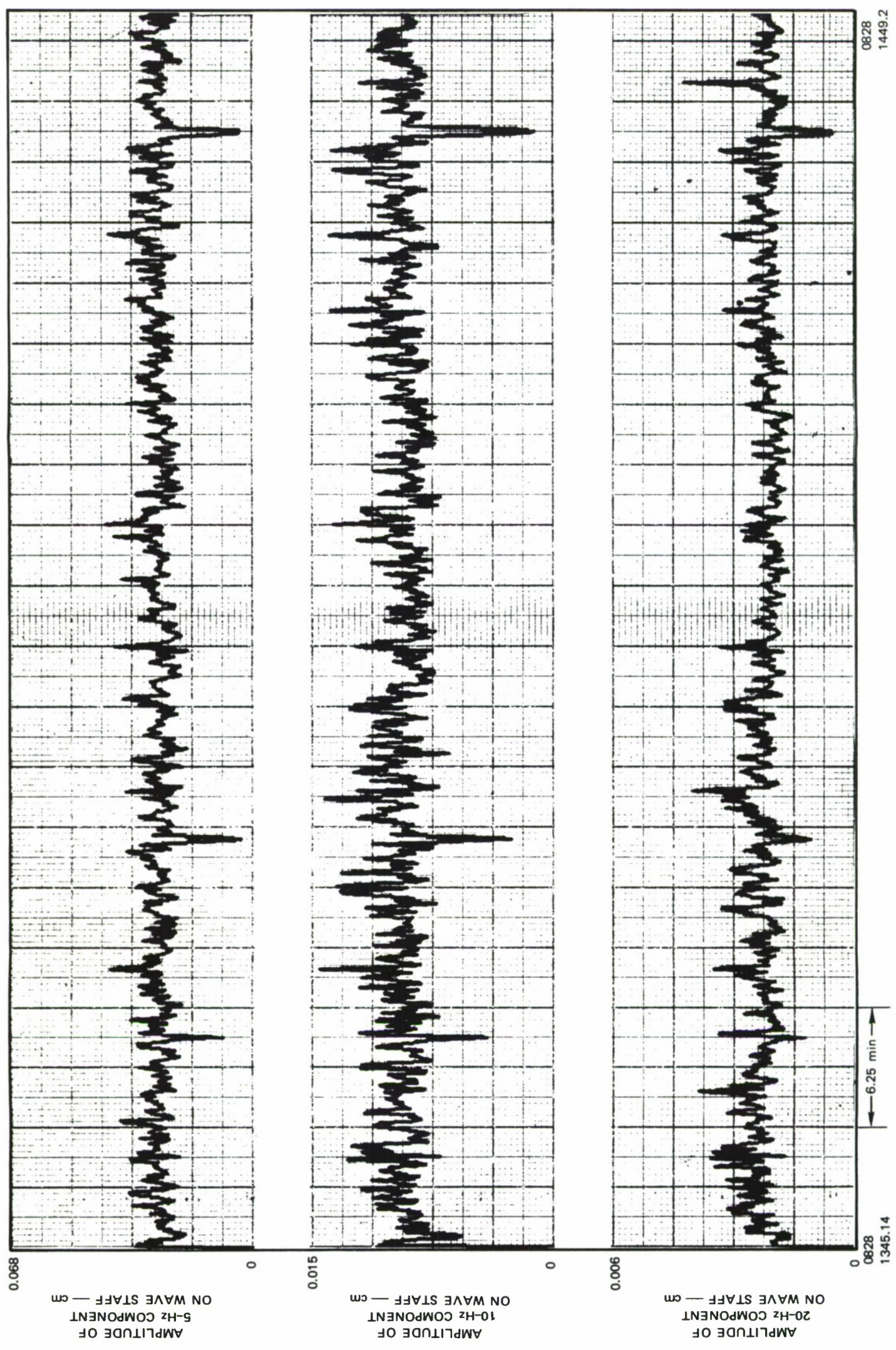


FIGURE 14 TEMPORAL DEPENDENCE OF WAVE HEIGHT AT DISCRETE FREQUENCIES FOR AUGUST 28 AT 1345.14

0828  
1345.14

1449.2  
→ 6.25 min →

0828  
1449.2

0828  
1449.2

0828  
1449.2

0828  
1449.2

0828  
1449.2

0828  
1449.2

0828  
1449.2

0828  
1449.2

0828  
1449.2

0828  
1449.2

0828  
1449.2

0828  
1449.2

0828  
1449.2

0828  
1449.2

0828  
1449.2

0828  
1449.2

0828  
1449.2

0828  
1449.2

0828  
1449.2

0828  
1449.2

0828  
1449.2

0828  
1449.2

0828  
1449.2

0828  
1449.2

0828  
1449.2

0828  
1449.2

0828  
1449.2

0828  
1449.2

0828  
1449.2

0828  
1449.2

0828  
1449.2

0828  
1449.2

0828  
1449.2

0828  
1449.2

0828  
1449.2

0828  
1449.2

0828  
1449.2

0828  
1449.2

0828  
1449.2

0828  
1449.2

0828  
1449.2

0828  
1449.2

0828  
1449.2

0828  
1449.2

0828  
1449.2

0828  
1449.2

0828  
1449.2

0828  
1449.2

0828  
1449.2

0828  
1449.2

0828  
1449.2

0828  
1449.2

0828  
1449.2

0828  
1449.2

0828  
1449.2

0828  
1449.2

0828  
1449.2

0828  
1449.2

0828  
1449.2

0828  
1449.2

0828  
1449.2

0828  
1449.2

0828  
1449.2

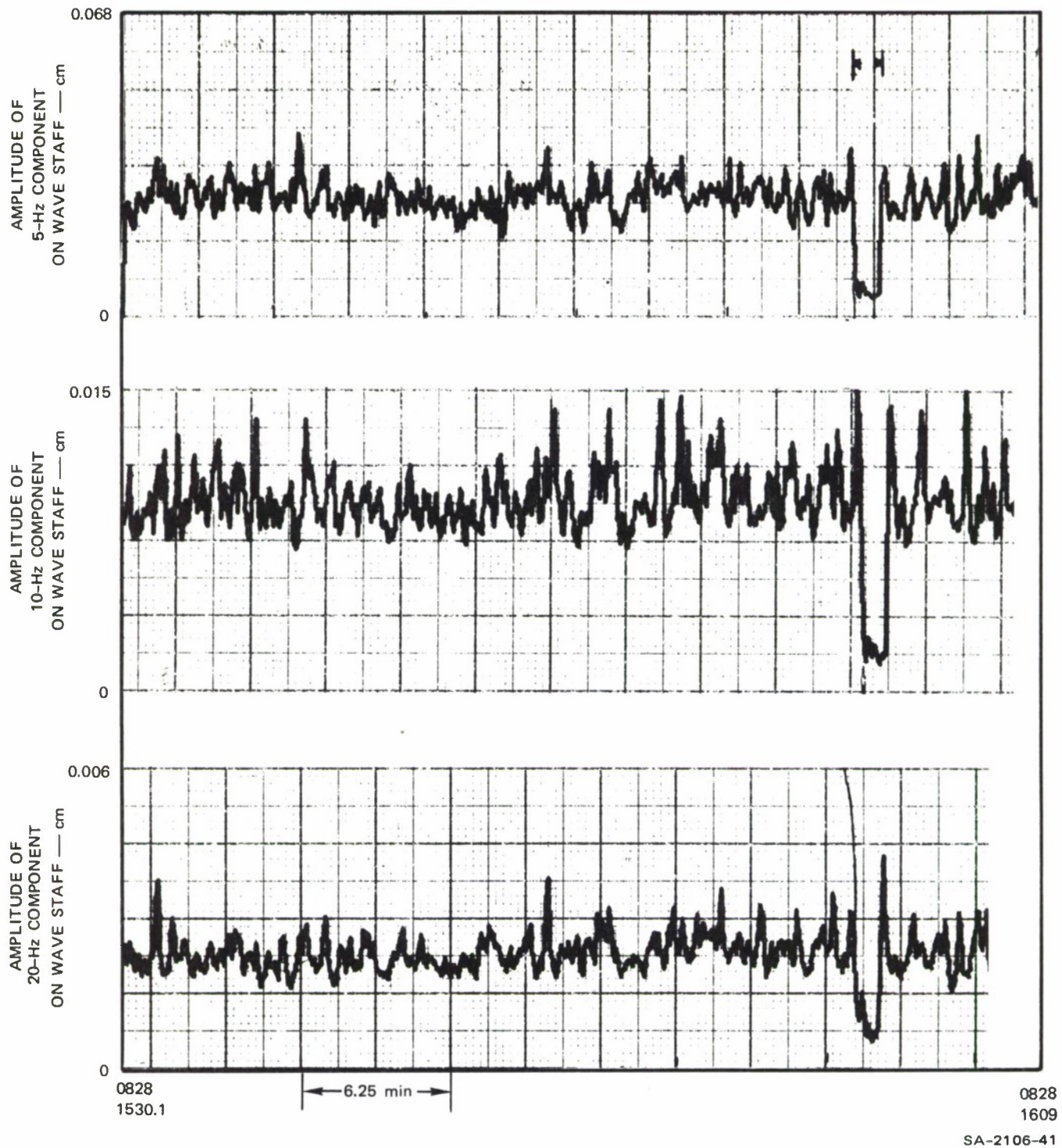


FIGURE 15 TEMPORAL DEPENDENCE OF WAVE HEIGHT AT DISCRETE FREQUENCIES FOR AUGUST 28 AT 1530.1

## B. Spatial Data Analysis

The time-average, or spatial-average fluctuations of the surface of the ocean can be described by a two-dimensional PSD function. In what follows, the one-dimensional PSD function inferred from the line of probes will be described.

The spatial PSD functions were calculated from the cross-correlation coefficients for each probe pair for zero time delay (averaged over 2.5 minutes). Six probes in a line sample the cross-correlation coefficient at 15 different separations. The 15 measurements were considered an adequate first step for determining the one-dimensional spatial PSD for a smoothly varying PSD function. To compute the spatial PSD from the measured data points, the correlation coefficients are constructed by linearly interpolating between measured points. To avoid a discontinuity in the spatial-correlation coefficient at the last point (a spacing of 50 cm), the correlation is smoothly decayed to negligible values with an exponential function having an e-folding distance of 100 cm--i.e., for  $\delta > 50$ ,  $R(\delta) = 1.65 R(50) \exp - (\delta/100)$ . This action has the effect of invalidating PSD estimates for wavelengths longer than 200 cm, but this is not serious since these wavelengths are of no interest in the present study.

A fast-fourier-transform (FFT) calculation of the spectrum was then made. Such a computation will generally contain negative estimates of energy at some wavenumbers. These are non-physical and are a consequence of measurement error and inadequate spatial sampling. To obtain a physically reasonable estimate of the PSD function, the initial PSD estimate is rectified and gaussian-weighted to smooth the correlation-function estimate. After rectification and weighting, an inverse transform is computed and the resulting correlation coefficient compared to the original measured correlation amplitudes. If the agreement is good, the weighted spectrum is taken as the "best" estimate of the spectrum, based on the measured correlations. If the fit is unsatisfactory, a

transform back to wavenumber space is undertaken and the gaussian weighting is modified. This trial and error procedure is carried out as often as required to obtain a good fit of the computed spatial correlation to the measured points. The spatial PSD corresponding to the "best-fitting" correlation function is taken as the "best" estimate of the spatial PSD function. An example of the result of this process is shown in Figure 16. The spatial PSD function is plotted against wavelength. The dashed straight line is a power-law fit to the computed PSD function. The inset in the upper right-hand corner shows the agreement between the measured correlations (shown by the squares) and the spatial correlation corresponding to the pictured PSD function. The lobing structure shown on the PSD plot has to do with the length of the correlation record and is a statistical quantity. The sensitivity of the computed spectra to changes in the spectral estimates has been estimated by multiplying the "best fit" spectrum by  $k^m$  where  $m$  was taken to be -1, -0.5, -0.25, +0.5, +0.25, and +1. Changes in  $m$  of 0.25 led to a significant degradation in the fit of the computed spatial correlation to the measured correlation, suggesting that the spectral estimates are valid to that order of exponent.

The spectra can be smoothed by averaging several spectra together. An average of five spectra was computed in this way. Some of these averaged spectra are shown in Figures 17 through 32. These figures represent 14.5-minute averages of the spectra (beginning at the time indicated in the lower left-hand corner). Clearly, further smoothing desirable. The best means of achieving this would be to reduce the averaging time associated with the first PSD estimate from 2.5 minutes to 10 seconds and then forming an average of as many spectra as necessary to achieve the desired smoothing.

On days of low wind, the apparent anomalous 5.5-Hz component that appears in some of the temporal PSD data increased in amplitude to

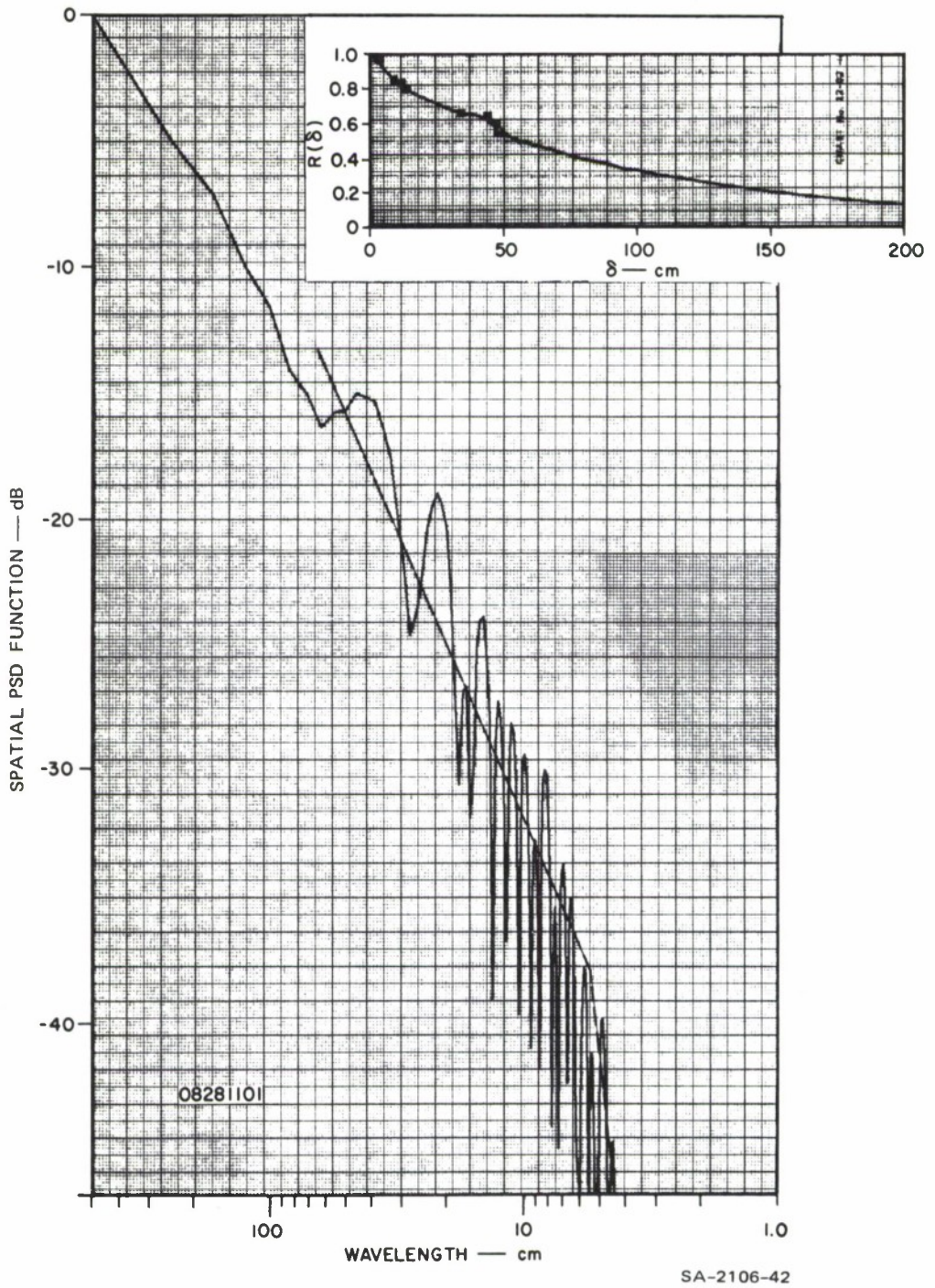


FIGURE 16 CALCULATED SPATIAL PSD FUNCTION FOR AUGUST 28 AT 1101  
(2.5-minute average)

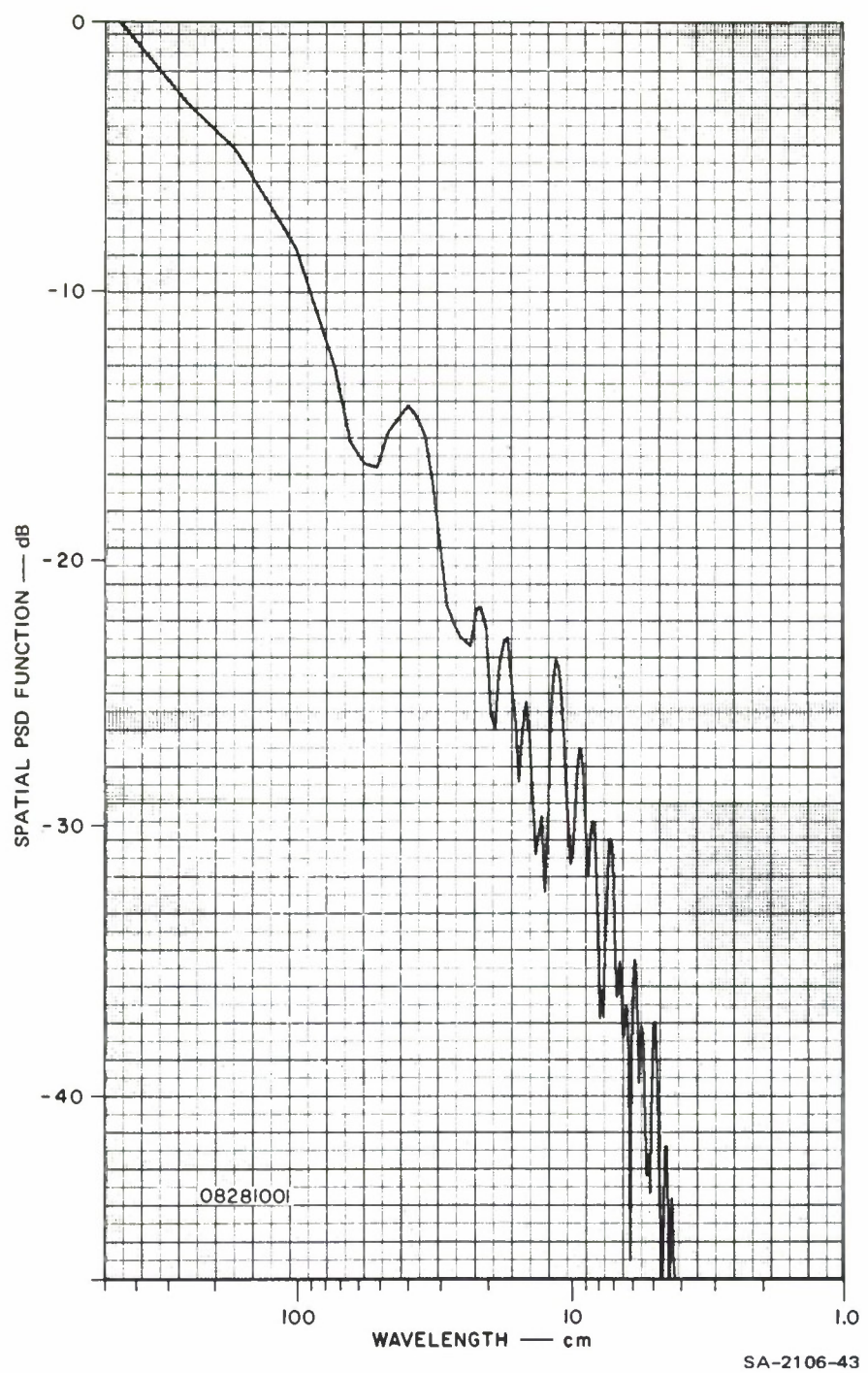


FIGURE 17 CALCULATED SPATIAL PSD FUNCTION FOR AUGUST 28 AT 1001.  
0 dB corresponds to  $65 \text{ cm}^2\text{-cm}$  (14.5 minute average).

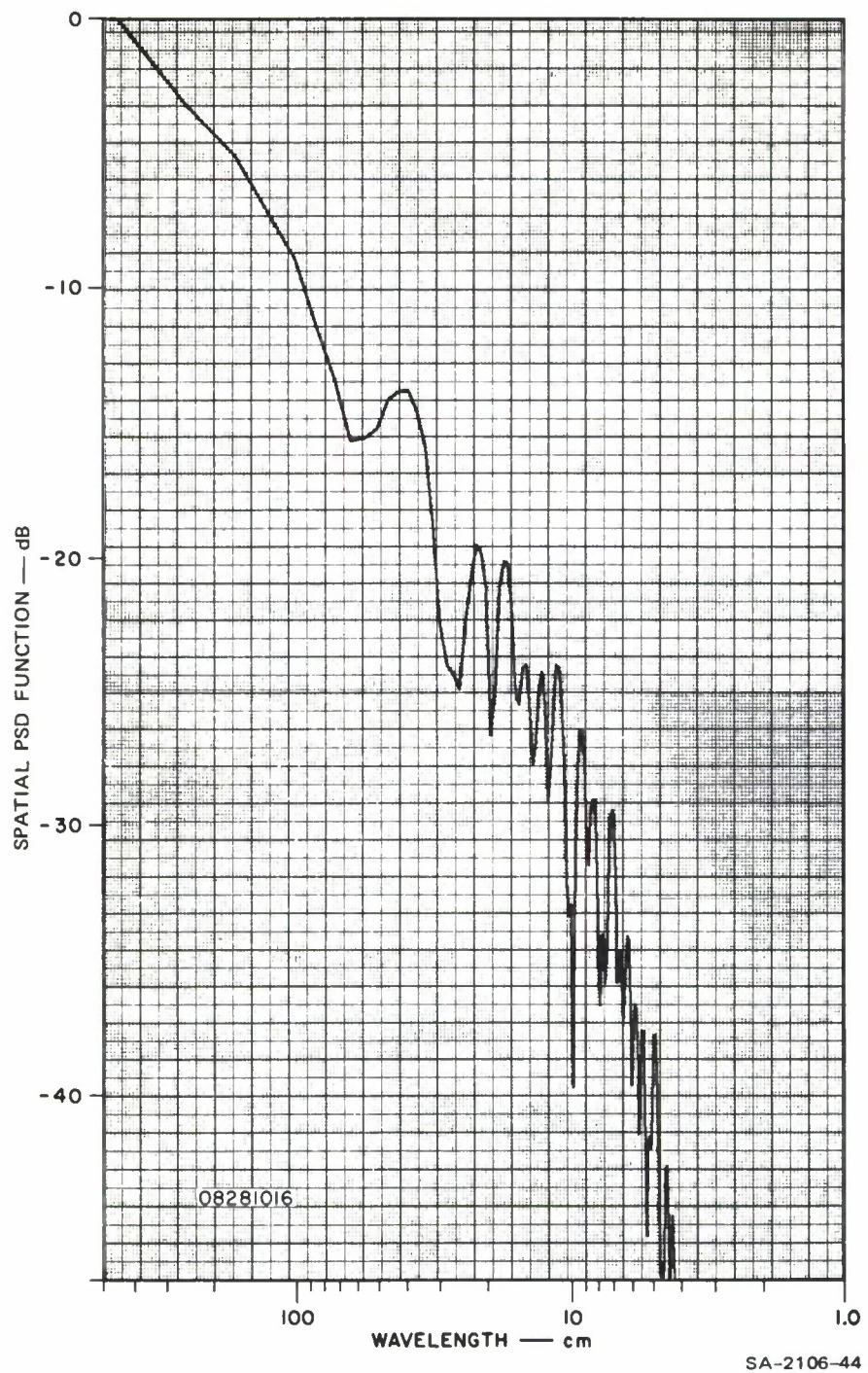


FIGURE 18 CALCULATED SPATIAL PSD FUNCTION FOR AUGUST 28 AT 1016.  
0 dB corresponds to  $72 \text{ cm}^2\text{-cm}$  (14.5 minute average).

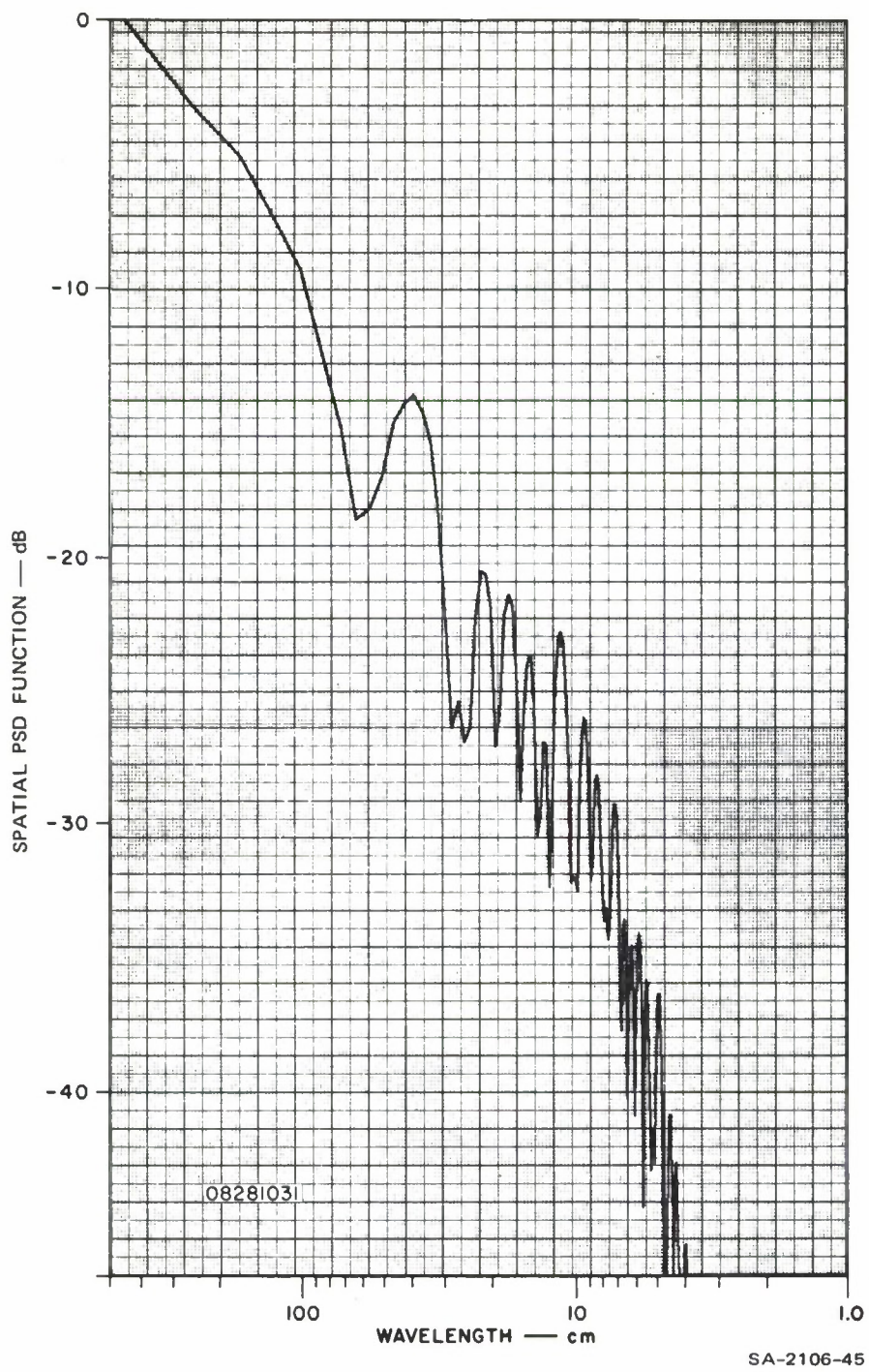


FIGURE 19 CALCULATED SPATIAL PSD FUNCTION FOR AUGUST 28 AT 1031.  
0 dB corresponds to  $89 \text{ cm}^2\text{-cm}$  (14.5 minute average).

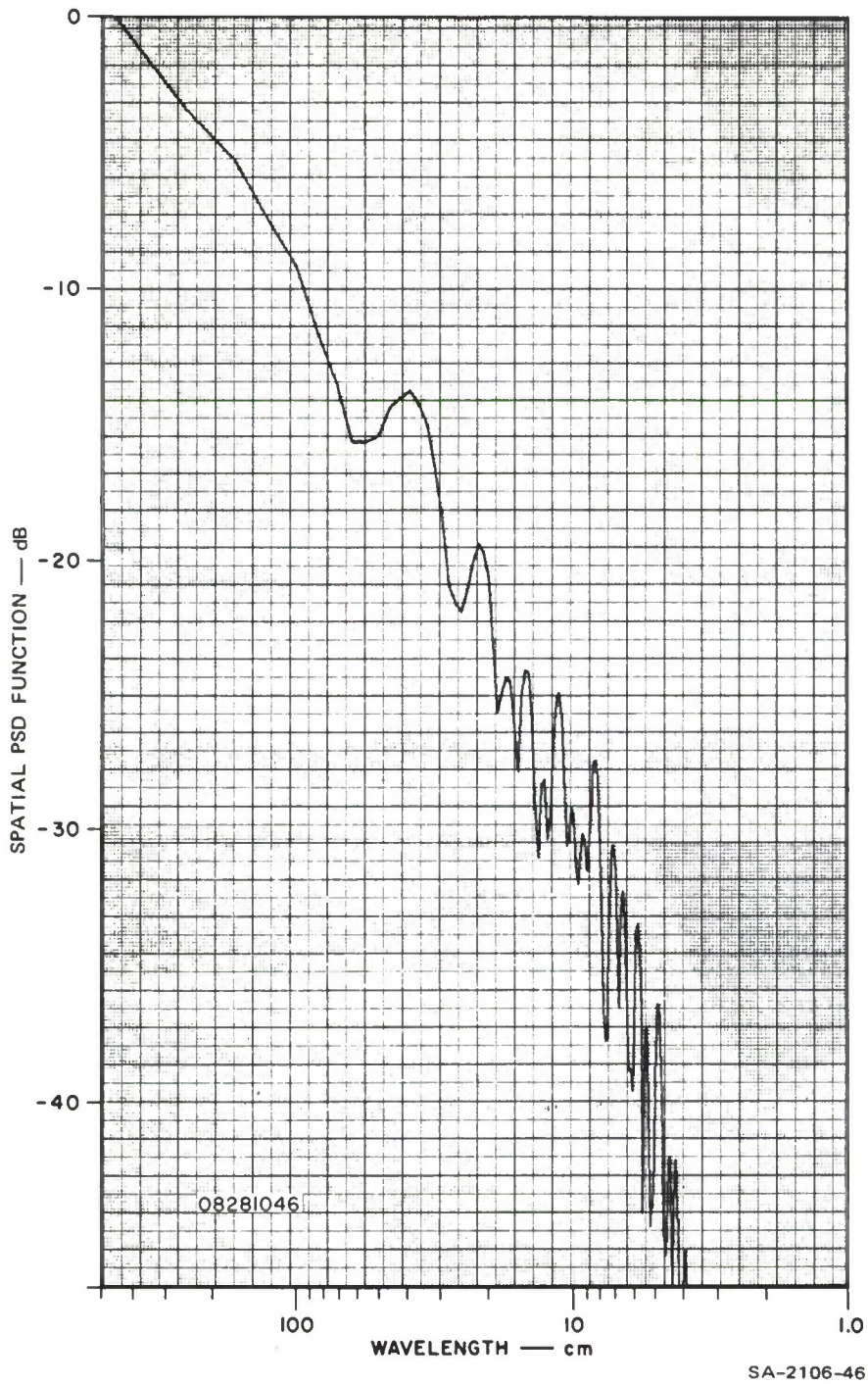


FIGURE 20 CALCULATED SPATIAL PSD FUNCTION FOR AUGUST 28 AT 1046.  
0 dB corresponds to  $88 \text{ cm}^2\text{-cm}$  (14.5 minute average).

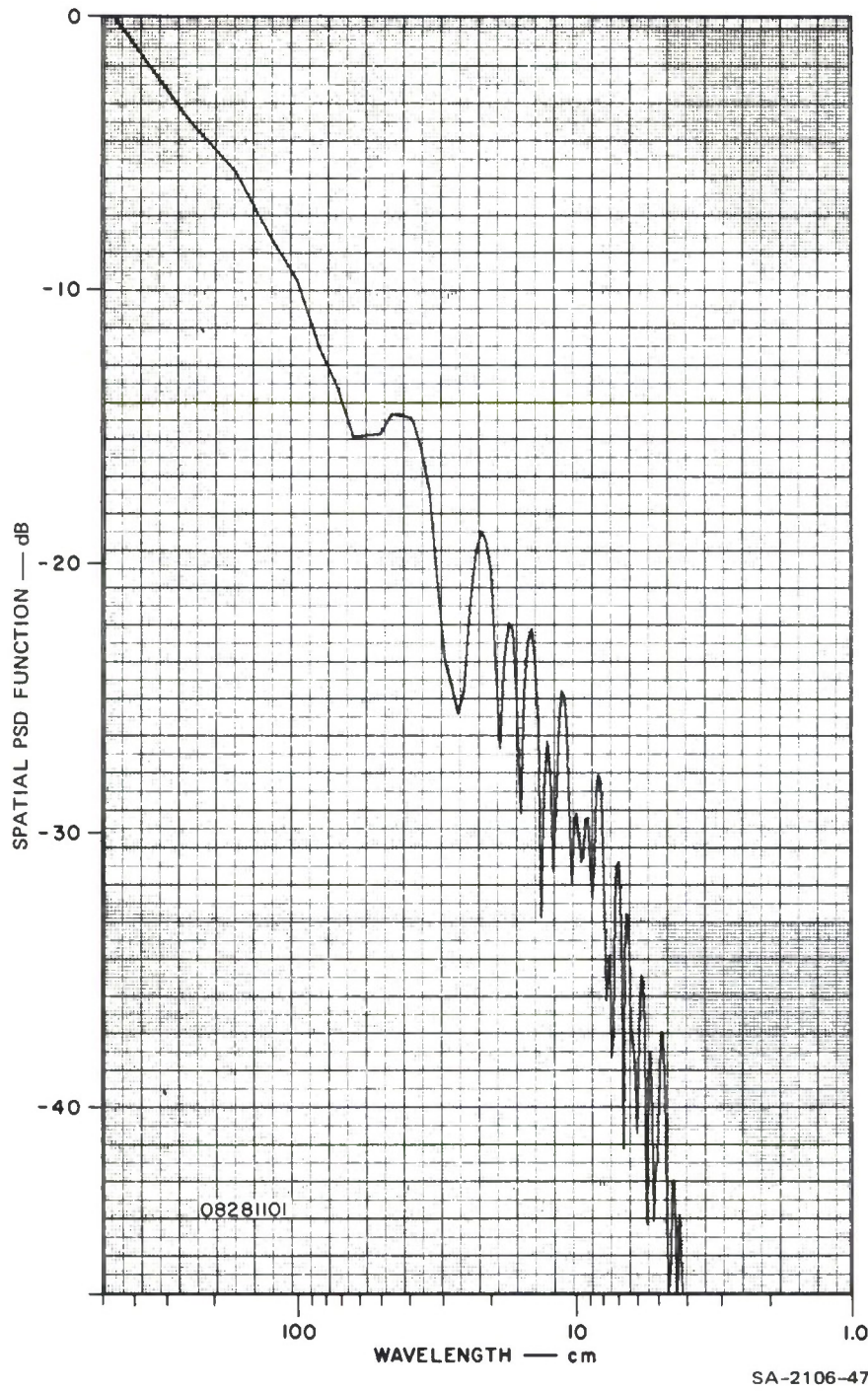


FIGURE 21 CALCULATED SPATIAL PSD FUNCTION FOR AUGUST 28 AT 1101.  
0 dB corresponds to  $93 \text{ cm}^2\text{-cm}$  (14.5 minute average).

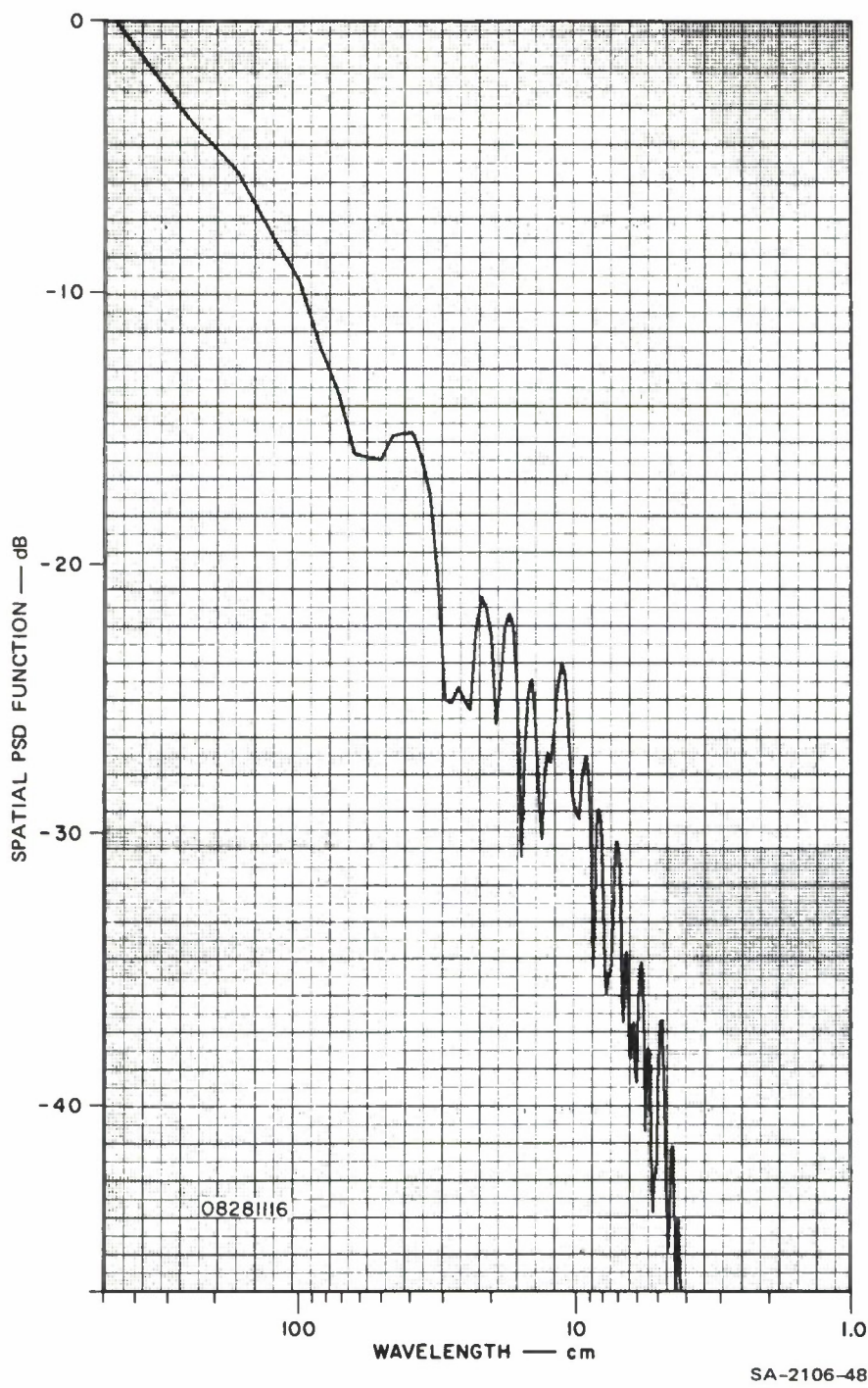


FIGURE 22 CALCULATED SPATIAL PSD FUNCTION FOR AUGUST 28 AT 1116.  
0 dB corresponds to  $93 \text{ cm}^2\text{-cm}$  (14.5 minute average).

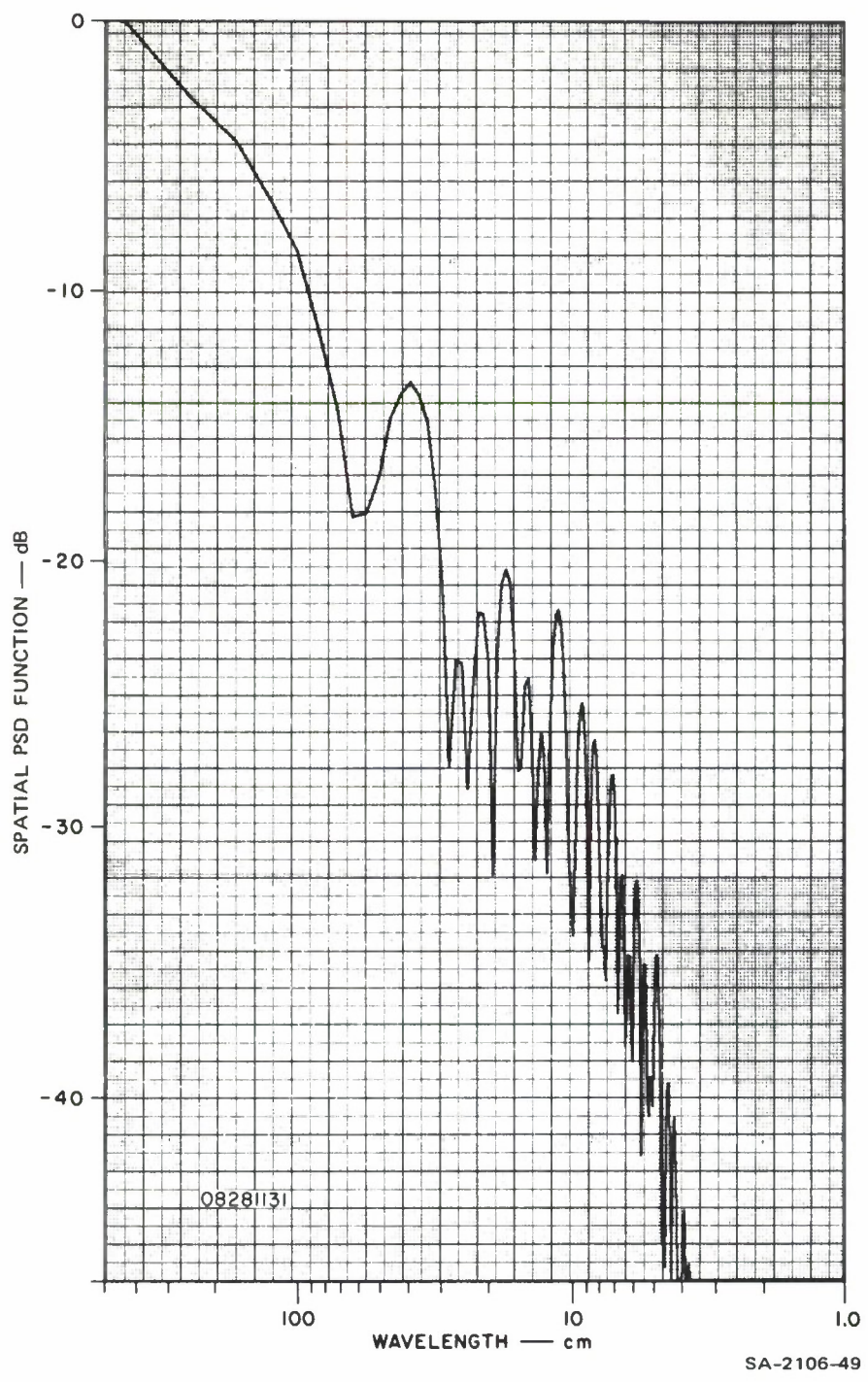


FIGURE 23 CALCULATED SPATIAL PSD FUNCTION FOR AUGUST 28 AT 1131.  
0 dB corresponds to  $76 \text{ cm}^2\text{-cm}$  (14.5 minute average).

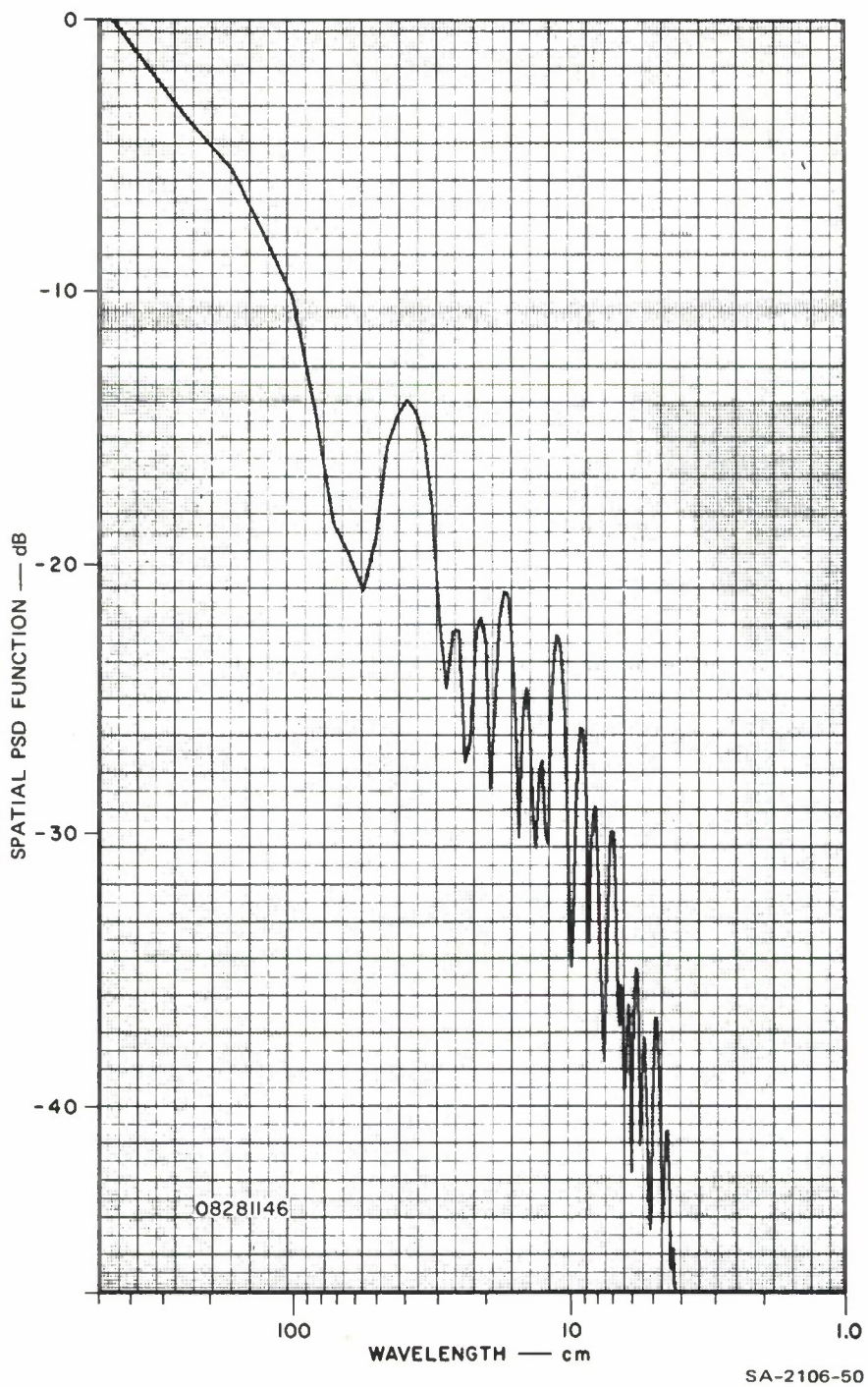


FIGURE 24 CALCULATED SPATIAL PSD FUNCTION FOR AUGUST 28 AT 1146.  
0 dB corresponds to  $69 \text{ cm}^2\text{-cm}$  (14.5 minute average).

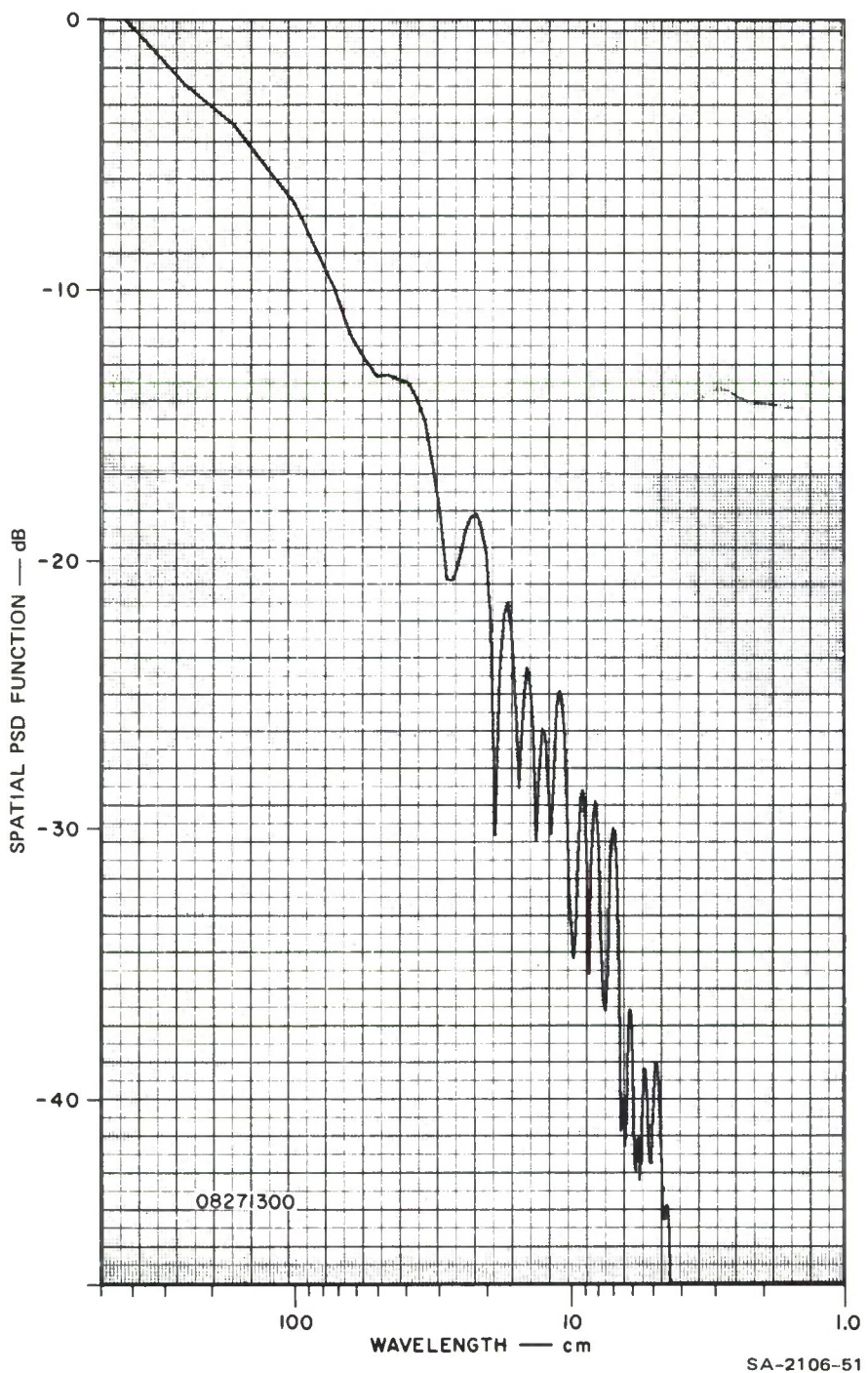


FIGURE 25 CALCULATED SPATIAL PSD FUNCTION FOR AUGUST 27 AT 1300.  
0 dB corresponds to  $23 \text{ cm}^2\text{-cm}$  (14.5 minute average).

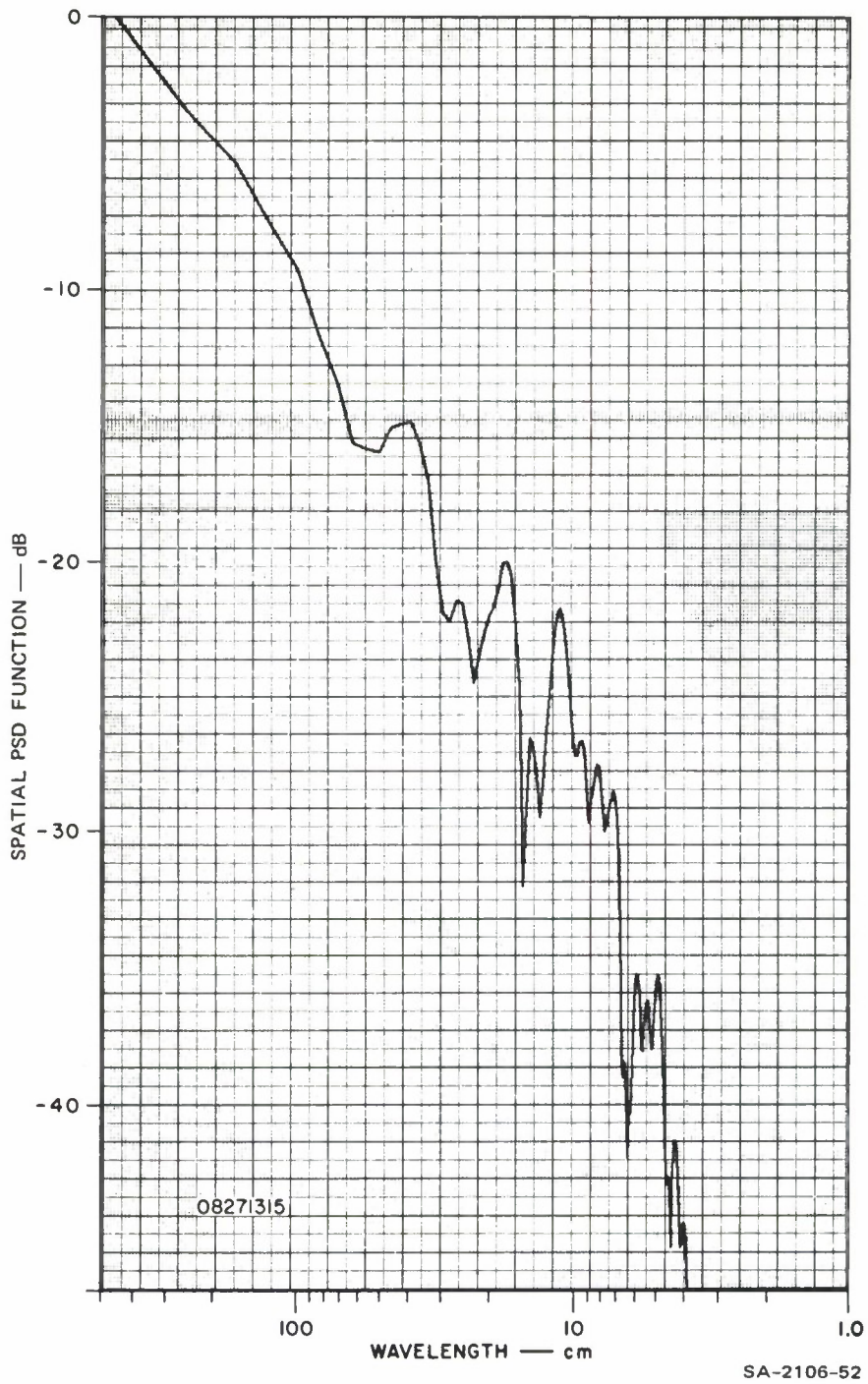


FIGURE 26 CALCULATED SPATIAL PSD FUNCTION FOR AUGUST 27 AT 1315.  
0 dB corresponds to  $46 \text{ cm}^2\text{-cm}$  (14.5 minute average).

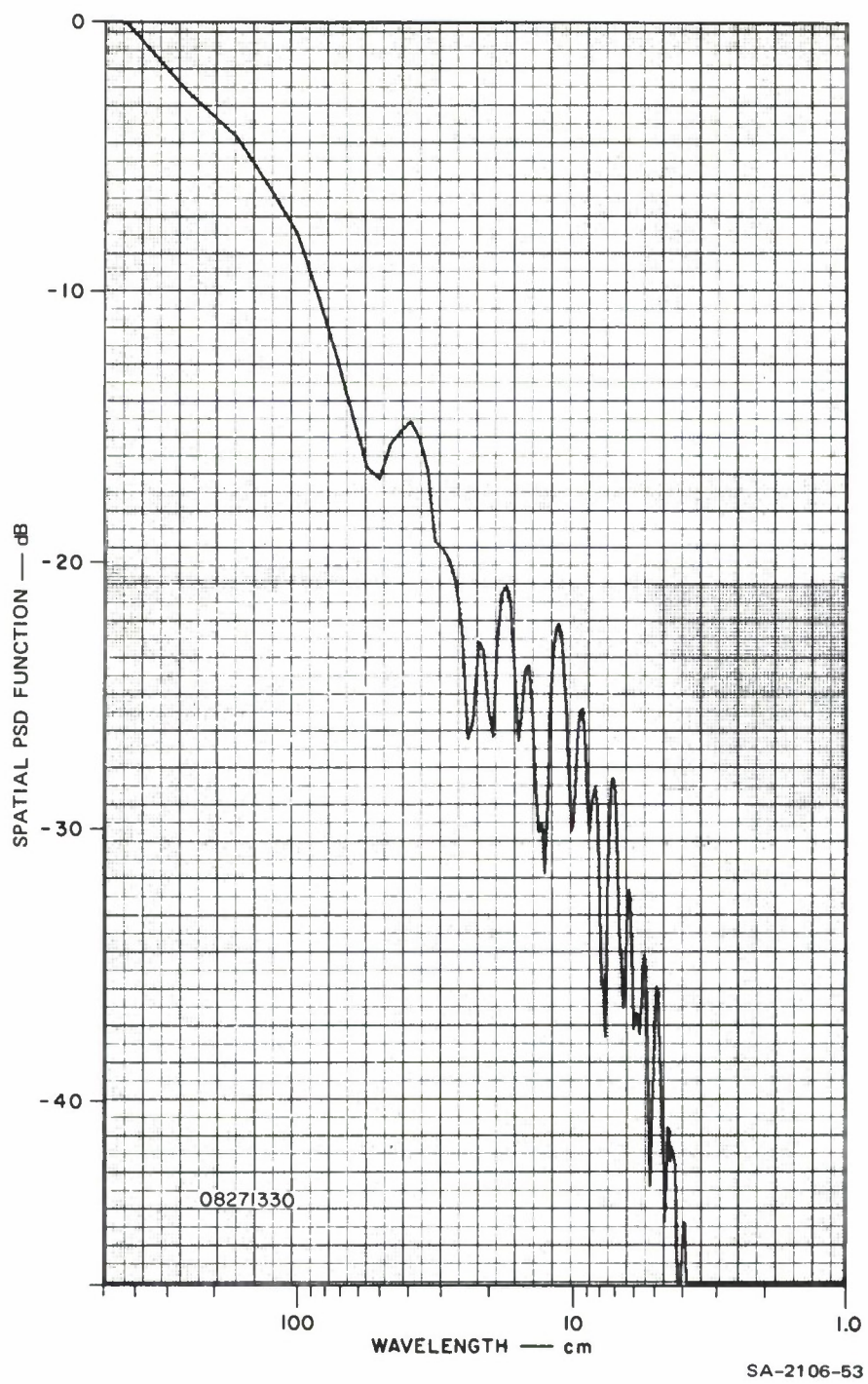


FIGURE 27 CALCULATED SPATIAL PSD FUNCTION FOR AUGUST 27 AT 1330.  
0 dB corresponds to  $36 \text{ cm}^2\text{-cm}$  (14.5 minute average).

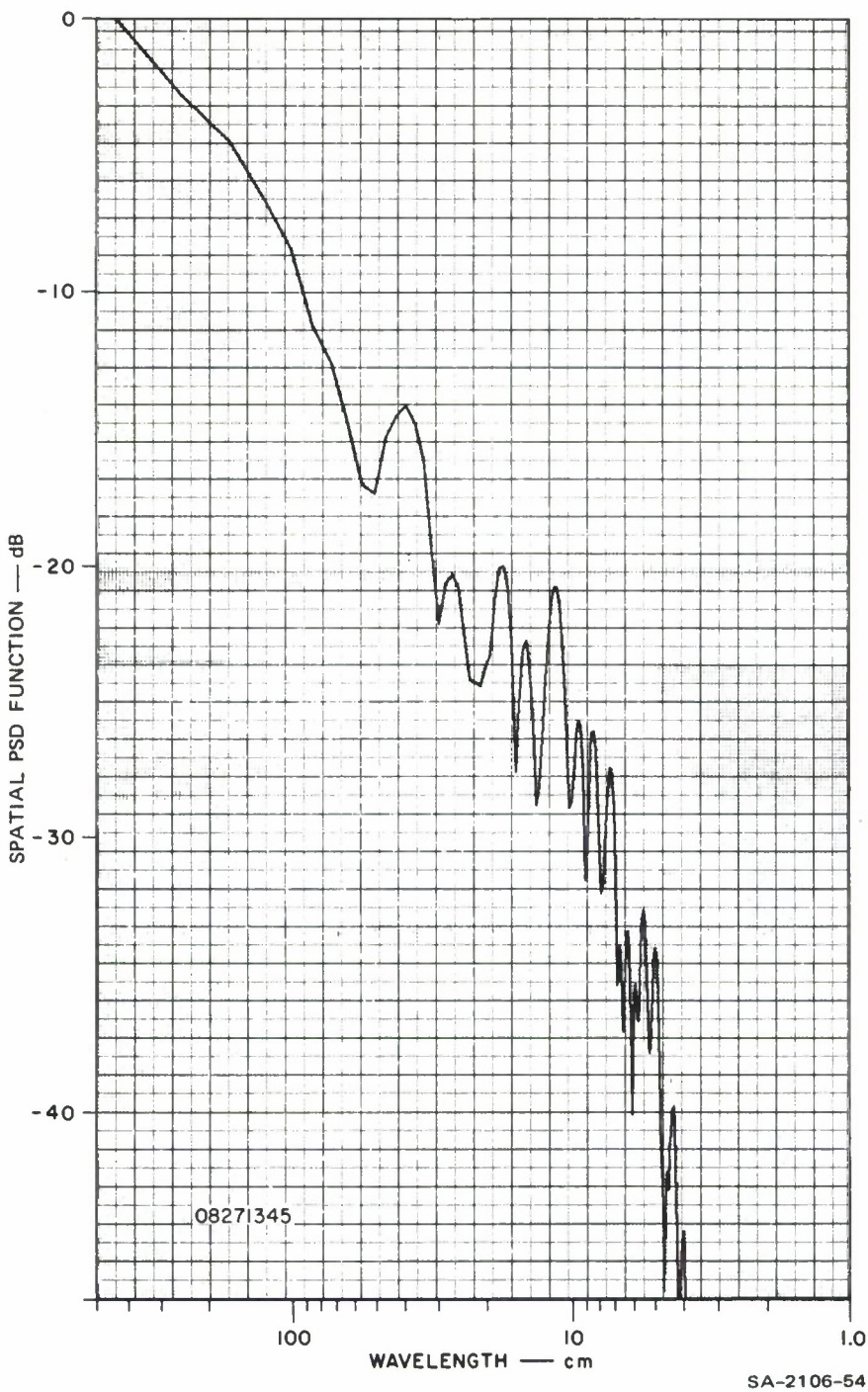


FIGURE 28 CALCULATED SPATIAL PSD FUNCTION FOR AUGUST 27 AT 1345.  
0 dB corresponds to  $35 \text{ cm}^2\text{-cm}$  (14.5 minute average).

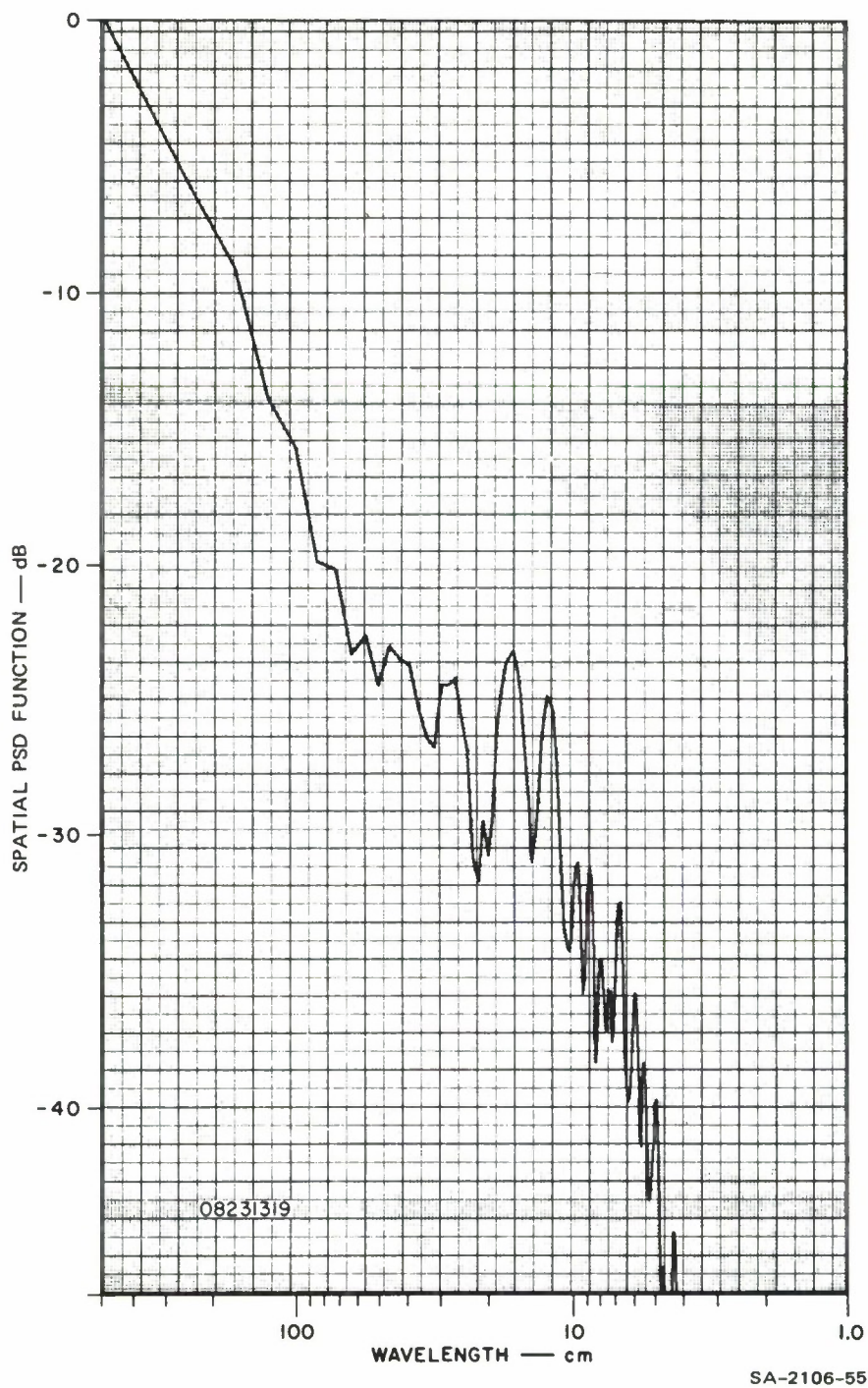


FIGURE 29 CALCULATED SPATIAL PSD FUNCTION FOR AUGUST 23 AT 1319.  
0 dB corresponds to  $38 \text{ cm}^2\text{-cm}$  (14.5 minute average).

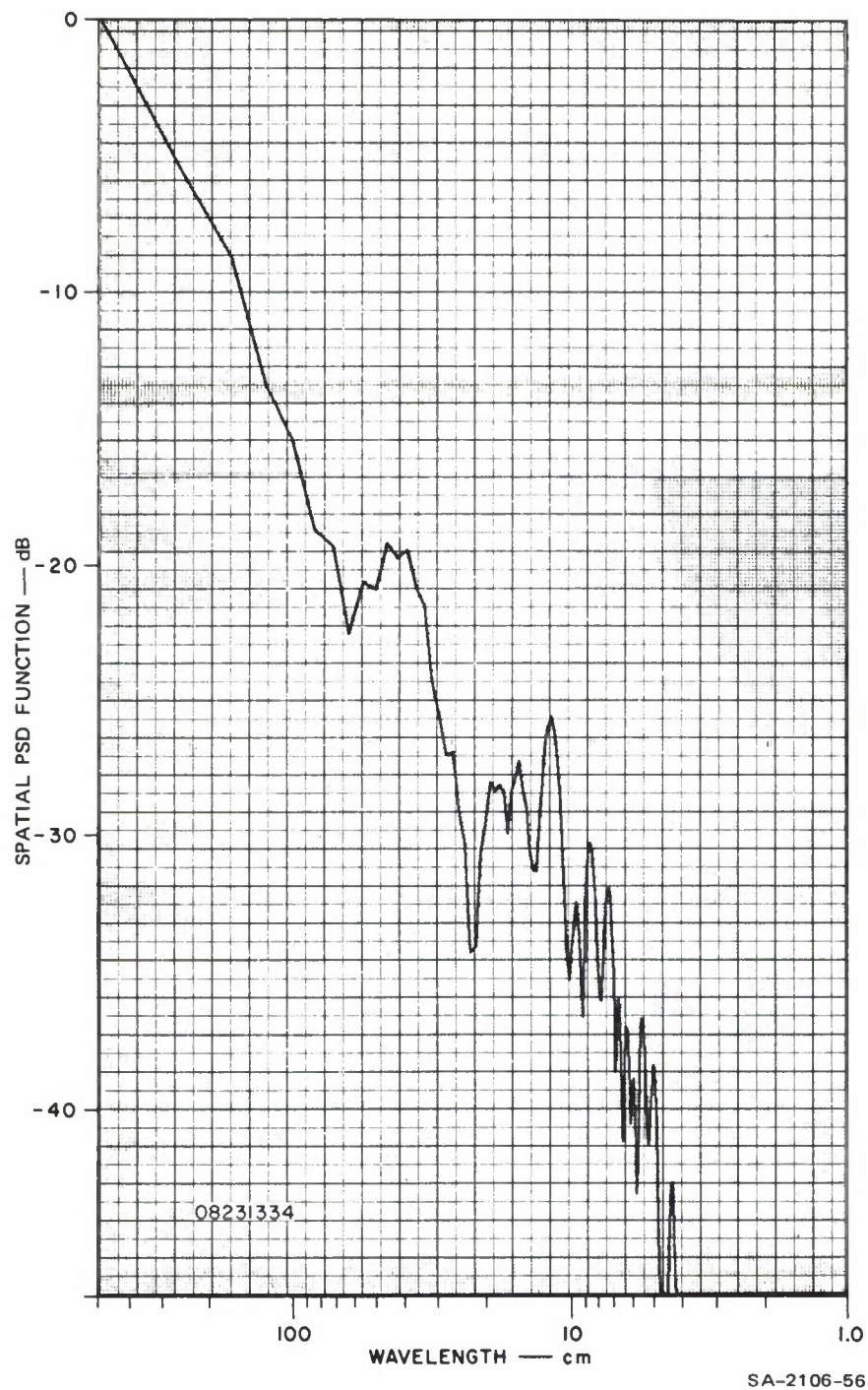


FIGURE 30 CALCULATED SPATIAL PSD FUNCTION FOR AUGUST 23 AT 1334.  
0 dB corresponds to  $48 \text{ cm}^2\text{-cm}$  (14.5 minute average).

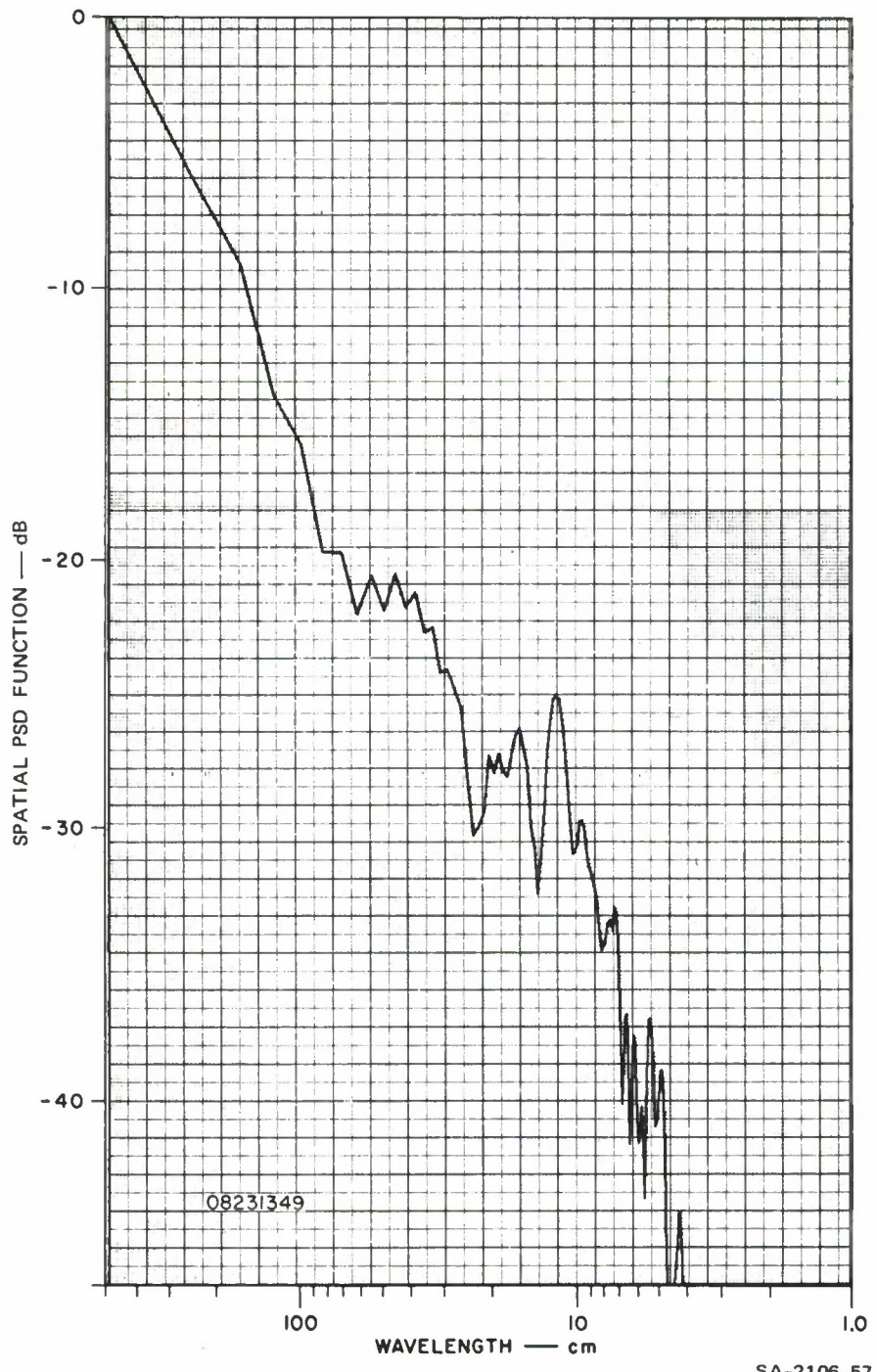


FIGURE 31 CALCULATED SPATIAL PSD FUNCTION FOR AUGUST 23 AT 1349.  
0 dB corresponds to  $38 \text{ cm}^2\text{-cm}$  (14.5 minute average).

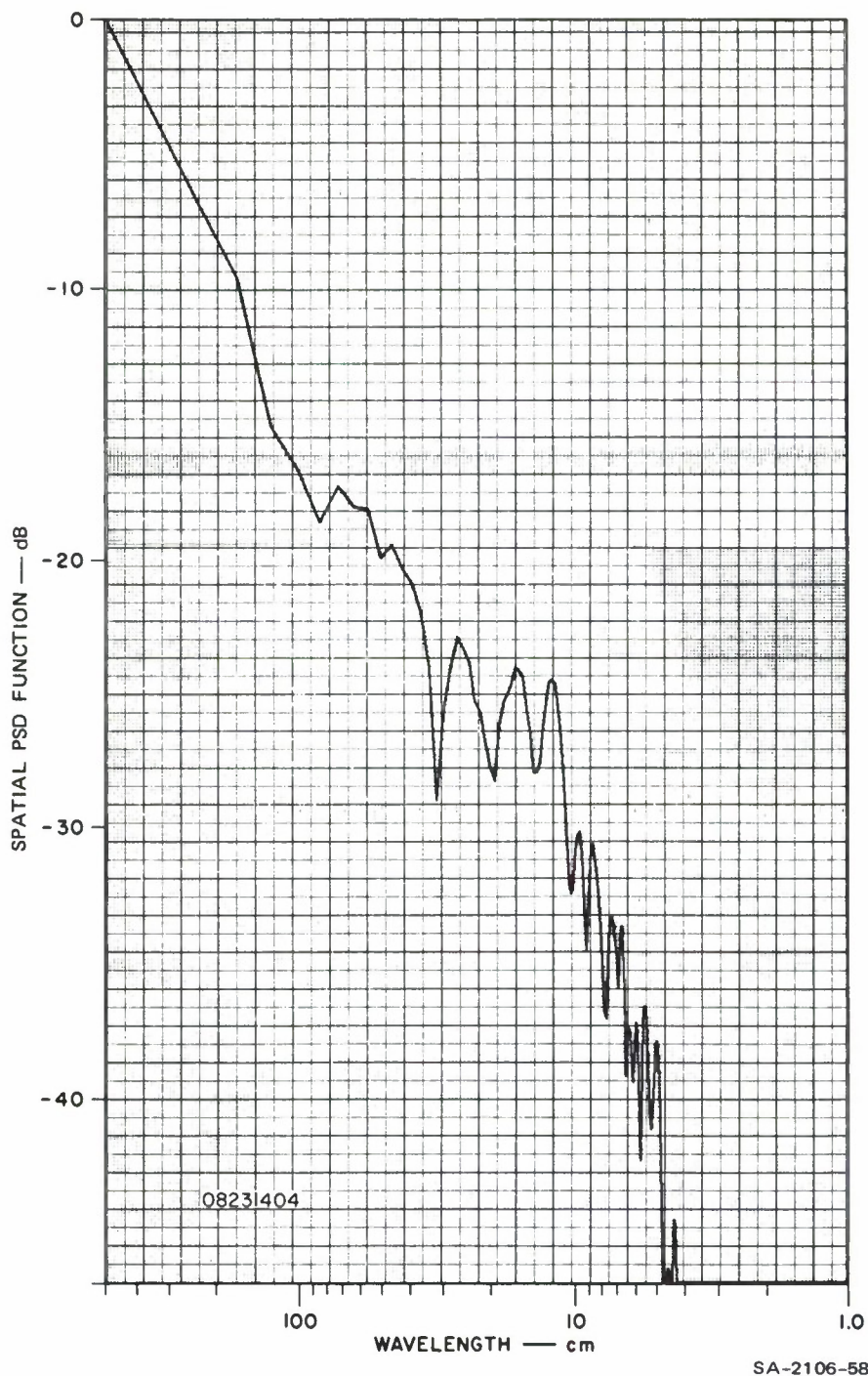


FIGURE 32 CALCULATED SPATIAL PSD FUNCTION FOR AUGUST 23 AT 1404.  
0 dB corresponds to  $40 \text{ cm}^2\text{-cm}$  (14.5 minute average).

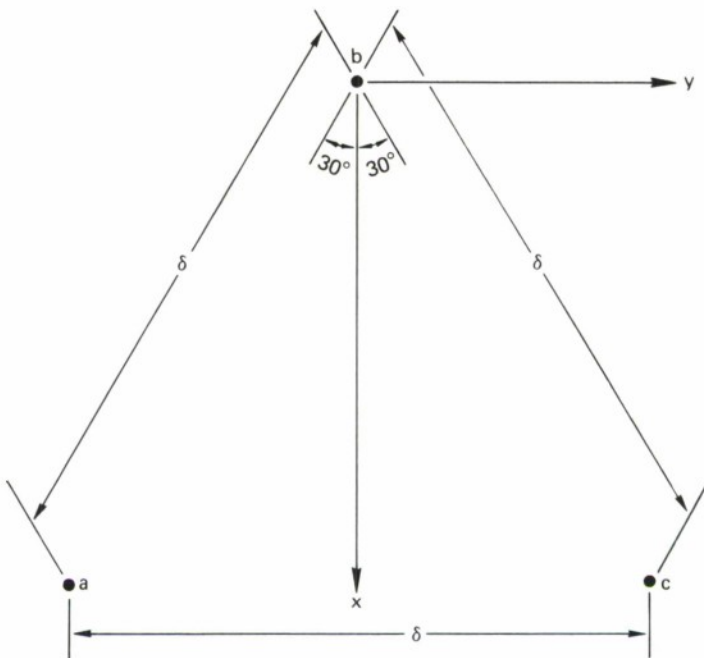
where it was only 5 dB below the peak amplitude. This strong monochromatic signal is evidenced in the measured spatial correlation by a strong periodicity that is seriously undersampled by the array. When spectral estimates of this kind of data were attempted, the quality of the inferred spatial PSD function was poor. It will be shown below that the observed 5.5-Hz component is a spurious reflection off the mechanical support for the cage. The difficulty in estimating spatial PSD functions for this condition is readily eliminated by filtering out the monochromatic component and repeating the calculation with the filtered data.

### C. Wave-Direction Finding

The direction of waves approaching the array can be inferred by measuring the phase on three probes separated as shown in Figure 33, and resolving the propagating waves into two orthogonal components. The relative phase measured on three probes provides three equations in two unknowns. The equations were solved for the components of the wavenumber, so that:

$$\begin{aligned}k_y &= (\varphi_{ab} + \varphi_{bc}) / (\delta \sin 30^\circ) \\k_x &= (\varphi_{bc} - \varphi_{ab}) / (\delta \cos 30^\circ) \\k_y &= \varphi_{ac} / \delta\end{aligned}$$

The direction of the incoming wave was inferred using phase data similar to those shown in Figure 7 and the foregoing equations. (The third and redundant equation was used as well to solve for wavenumber, and it gave results consistent with the estimate determined from the first two equations.) Table 1 shows the directions from which waves were coming for a number of selected times. It was further observed that, in some instances, the lower- and higher-frequency waves were not coming from the same direction.



$$-k_x \delta \cos 30^\circ + k_y \delta \sin 30^\circ = \varphi_{ab}$$

$$k_x \delta \cos 30^\circ + k_y \delta \sin 30^\circ = \varphi_{bc}$$

$$k_x \delta = \varphi_{ac}$$

WHERE  $k_x$  AND  $k_y$  ARE COMPONENTS OF THE PROPAGATING WAVE

SA-2106-59

FIGURE 33 DIRECTION-FINDING FORMALISM

It was previously observed in the temporal spectra that an identifiable 5.5-Hz component exists in nearly all the data. The direction-finding formalism was used to identify the source of this component. It was determined that this wave was emanating from the mechanical support rods of the wave-staff array. It was further determined that the 5.5-Hz reflected wave propagates at the velocity predicted by the wave-dispersion relation.

By way of contrast to the foregoing, the rate of change of phase with frequency of the wind-driven ocean waves is observed to be very nearly linear. This result is inconsistent with the wave-dispersion relation for one-dimensional waves. Wind-wave-tank measurements<sup>1</sup> of

1. H. Guthart, W. C. Taylor, K. A. Graf, and D. G. Douglas, "Correlation Techniques and Measurements of Wave-Height Statistics," Final Report, SRI Project 1183, Contract NAS1-10681, Stanford Research Institute, Menlo Park, Calif. (May 1972).

Table 1  
INFERRRED WAVE DIRECTIONS

Date and Time	Direction (degrees)
08231343	192
08231413	194
08271012	303
08271042	330
08271115	320
08271145	330
08271215	322
08271245	330
08271315	330
08271345	330
08271545	330
08271615	330
08281013	338
08281043	337
08281113	332
08281345	340
08281415	337
08281545	340
08301544	211
08301614	197

the phase frequency characteristic have been observed to have a similar linear behavior. The observed characteristic is perhaps a consequence of the harmonic content of the waves. In this case, the linearity of

the phase-frequency characteristic indicates that the propagation of these waves is nondispersive. Alternatively, the observed linear characteristic might be a consequence of the variability of wave direction.

In using the direction-finding formulas for determining wave direction, the magnitude of wavenumber corresponding to each frequency can be determined ( $|k| = \sqrt{k_x^2 + k_y^2}$ ), so that the frequency and wavenumber relationship can be determined. This computation affords a potential means for using temporal spectra and the phase data to determine spatial spectra. If this analysis can be exploited, spatial spectra should be determinable to a high degree of accuracy with very few wave staffs.

It has also been inferred that 29 Hz corresponds to wavelengths considerably longer than 1 cm, so that the foregoing data analysis undersampled the data if the shortest wavelength to be measured was 1 cm. This conclusion was confirmed by studying the spatial spectra of Figures 17 through 32, where the spectra roll off at wavelengths considerably longer than 1 cm. The undersampling is readily circumvented by redigitizing the analog data at higher frequencies.

### III CAPILLARY-WAVE-ATTENUATION SENSOR

Early in August, SRI undertook the development of a capillary-wave attenuation sensor. This instrument is intended to measure the spatial-attenuation factor leading to an estimate of surface tension. The instrument that was constructed generated a water wave by vertically oscillating a 6.3-cm-diameter cylinder at a 20-Hz rate. The generated wave amplitude was then measured at three distances from the cylinder by resistance-type wave staffs (of 0.0025 cm diameter). A schematic diagram of the instrument is shown in Figure 34. To inhibit the propagation of naturally occurring 20-Hz waves, two faces of the instrument were screened. The rate at which surface water replaced itself was not measured during the short time available for the development of the instrument. The attenuation factor is inferred from the ratios of the measured amplitudes squared using a cylindrical-wave approximation of the form

$$\left(\frac{V_1}{V_2}\right)^2 = r_2 \frac{e^{-2\alpha(r_1 - r_2)}}{r_1} \quad (1)$$

where the V designates the measured voltage, r is the radial dimension from the apparent source of the wave,  $\alpha$  is the spatial-attenuation factor, and the subscripts 1 and 2 designate the probe number. Equation (1) is readily solved for the attenuation factor  $\alpha$ , so that

$$\alpha = \frac{-1}{2(r_1 - r_2)} \ln \left[ \left( \frac{r_1}{r_2} \right) \left( \frac{V_1}{V_2} \right)^2 \right] . \quad (2)$$

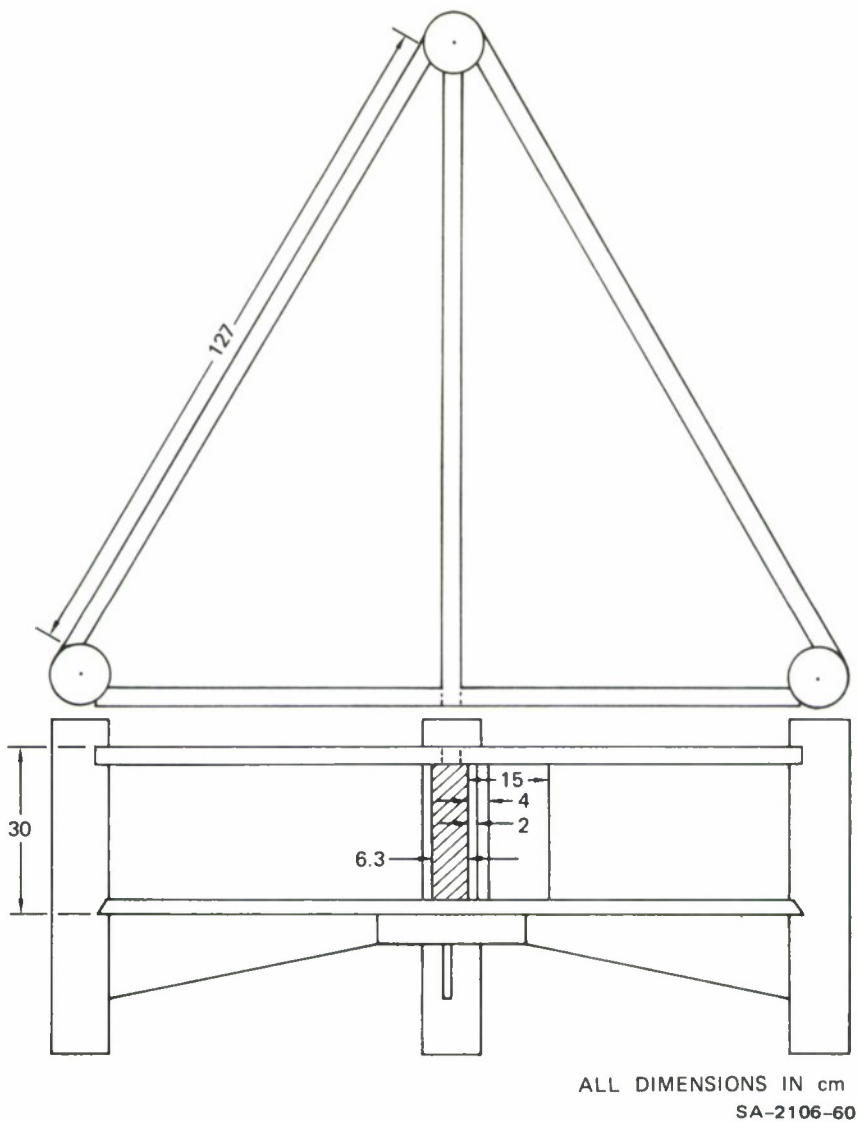


**FIGURE 34 SCHEMATIC OF CAPILLARY-WAVE-ATTENUATION SENSOR**

The capillary-wave-attenuation sensor was deployed at the tower on August 29, 1972, and on the succeeding two days. Approximately 15 hours of data were recorded with this instrument. It was deployed 30 m north of the northeast leg of the tower. Figure 35 shows the inferred spatial-attenuation factor for selected times during the three days. The averaging time of these data is one minute. The data were resampled for 15-second averaging times and the results were not significantly different. The insensitivity of the results suggest that the time required to replace the water in the instrument was comparable to, or exceeded, one minute.

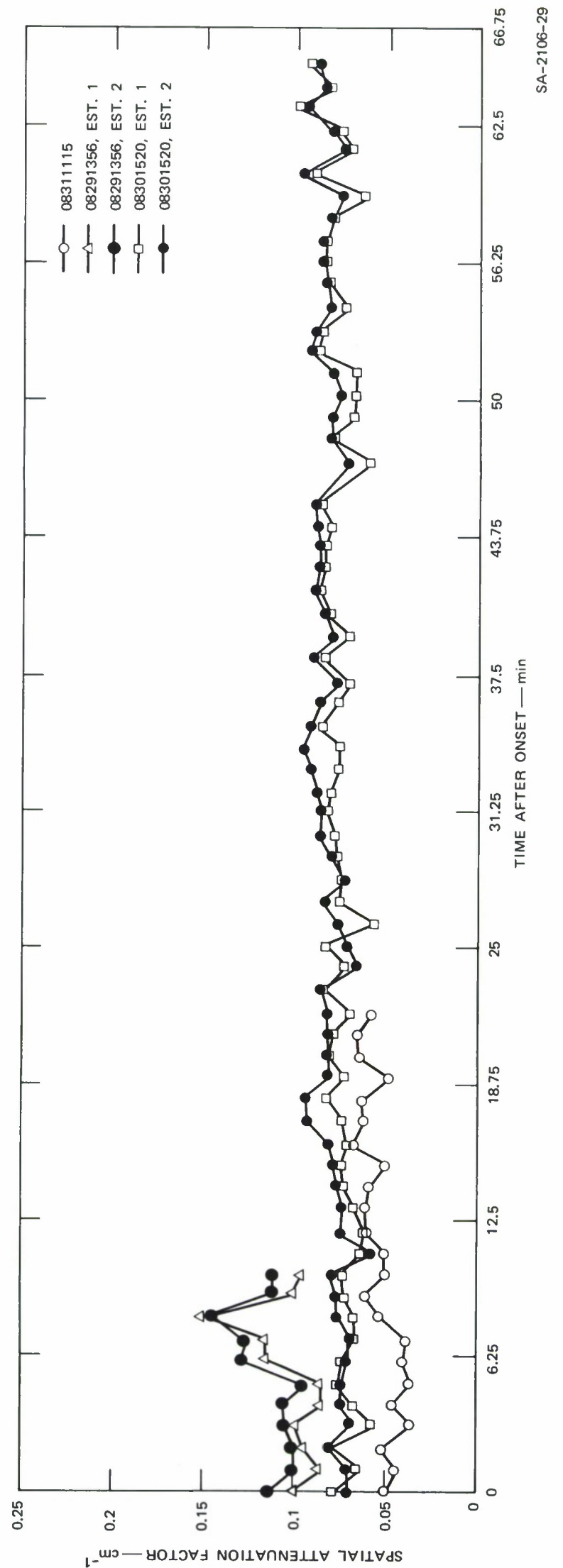


FIGURE 35 MEASURED SPATIAL-ATTENUATION FACTOR

SA-2106-29

The amplitude of the inferred spatial-attenuation factor suggests that the water in the vicinity of the tower is only moderately dirty (clean water has an attenuation factor of  $0.032 \text{ cm}^{-1}$ ).

#### IV MICROWAVE RADIOMETER

A microwave radiometer senses the thermal emissions of the ocean surface. The measured radiometric temperature,  $T_R$ , is equal to the product of the surface emissivity,  $\epsilon$ , and the water temperature, T--i.e.,

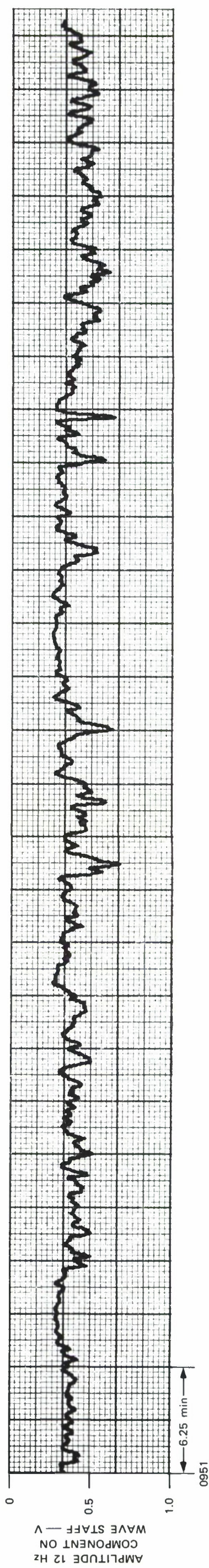
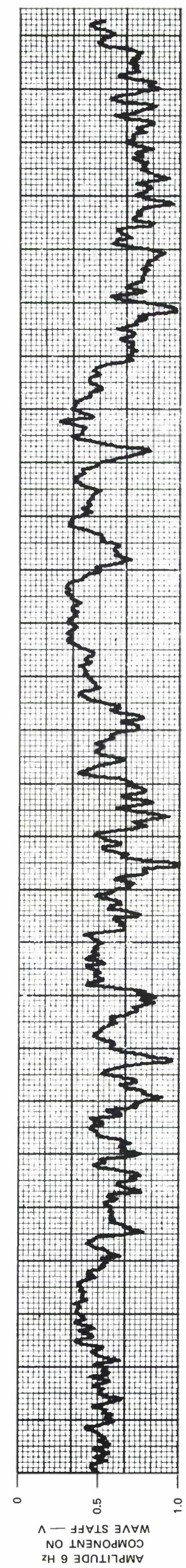
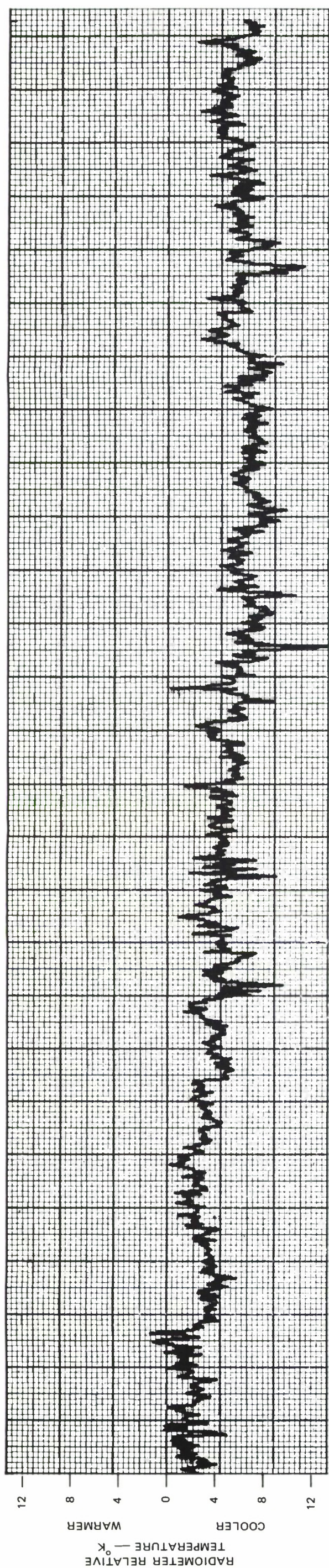
$$T_R = \epsilon T . \quad (3)$$

The emissivity of the surface is in turn dependent on the surface statistics, microwave wavelength, polarization, and angle of incidence. At most microwave frequencies of interest the reflective sky radiation is a negligible contributor to the radiometric temperature.

SRI has a null-type Dicke radiometer at 8.9 GHz, which was fielded at the NUC tower at no expense to the sponsor. Forty hours of data were recorded in the period August 24 through August 31. The radiometer look at the sea surface a few meters due east of the wave-staff array with a resolution cell having a diameter of approximately 3 meters.

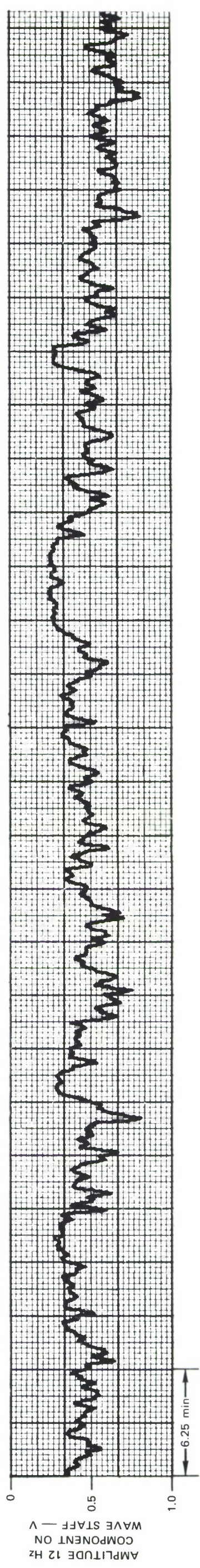
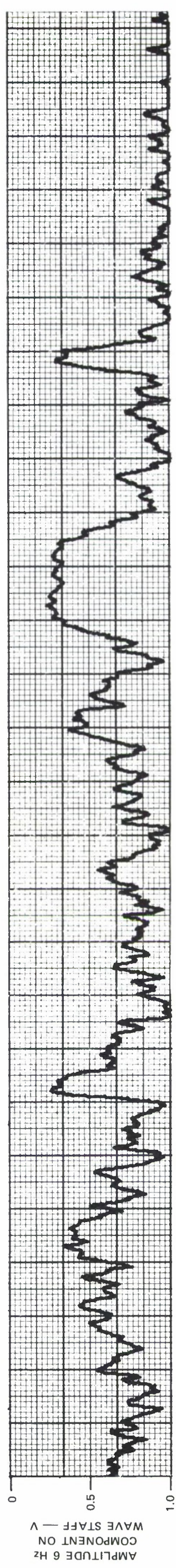
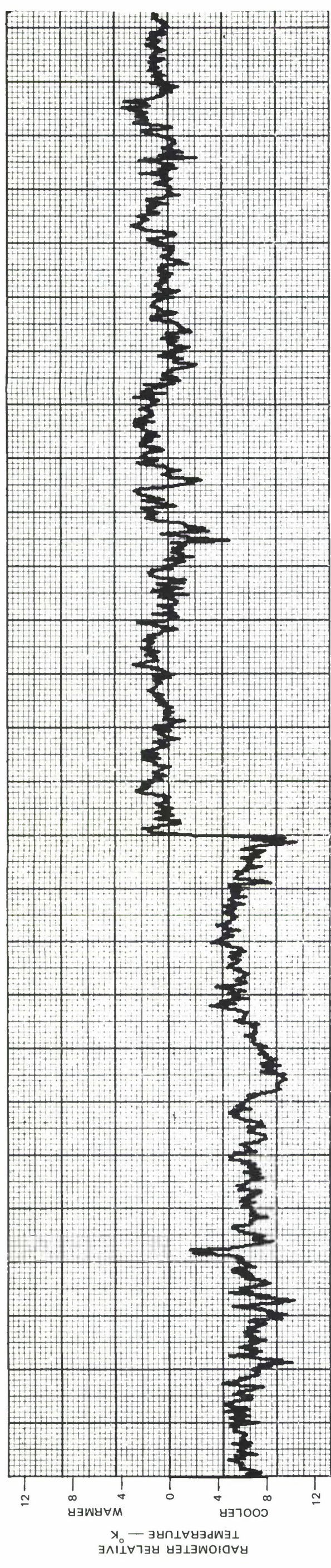
Figures 36 through 46 show the measured radiometric fluctuations as a function of time. These figures also show, to the same scale, the amplitude of the 6-Hz and 12-Hz components derived from one of the resistance wave staffs. Theory would dictate that decreasing wave-height fluctuations (a rising curve in these figures) would produce an apparently cooler radiometric temperature. To verify this hypothesis, the measured radiometric fluctuations were cross correlated with the amplitude of the 6-Hz and 12-Hz wave components for each record (as depicted in Figures 36 through 46). The ensemble of 11 records was then averaged with the results shown in Figure 47 (for the 6-Hz correlation) and Figure 48 (for

the 12-Hz correlation). It is seen from these figures that the correlation between wave-height fluctuations and radiometric temperature is significant (i.e., well above the noise level). It is difficult to predict the magnitude of the correlation to be expected because the wave staff is a point sensor, whereas the radiometer is an area sensor, and the wave staff is sensing a discrete wavenumber, whereas the radiometer effectively integrates over a wavenumber band. The correlation between the radiometer output and the discrete surface-wave frequencies is comparable at both frequencies. The correlation readily demonstrates the sensitivity of radiometric fluctuations to surface-height fluctuations, suggesting the suitability of microwave radiometry as a remote sensor of the sea surface.



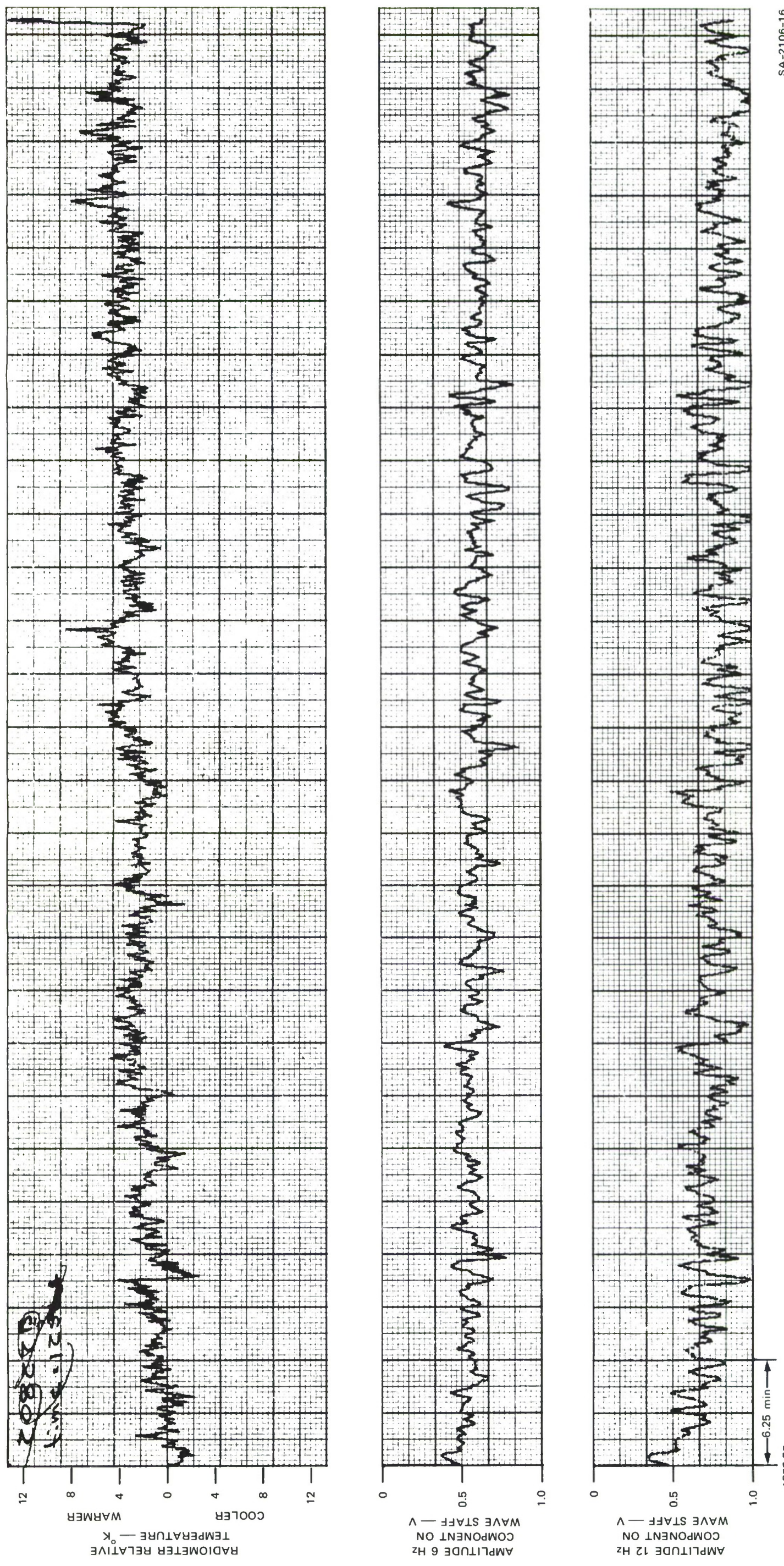
SA-2106-14

**FIGURE 36** TEMPORAL DEPENDENCE OF  
RADIOMETER AND BAND-  
LIMITED WAVE-STAFF  
OUTPUTS FOR AUGUST 27  
BEGINNING AT 0951.0

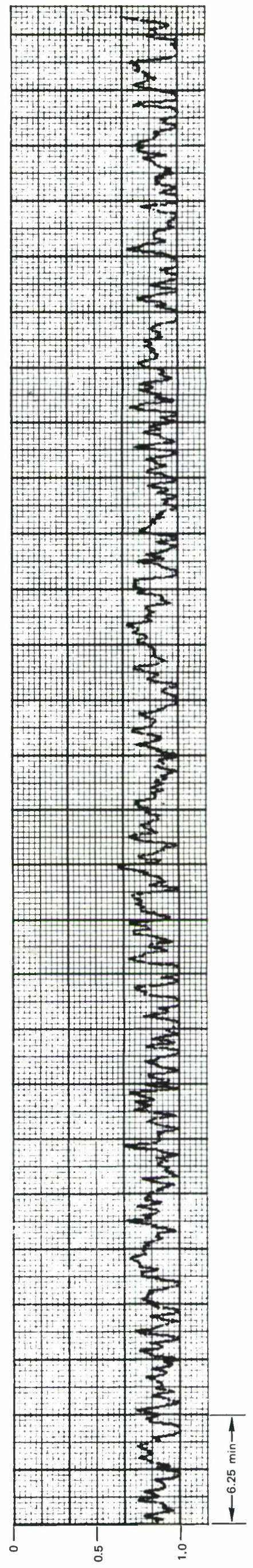
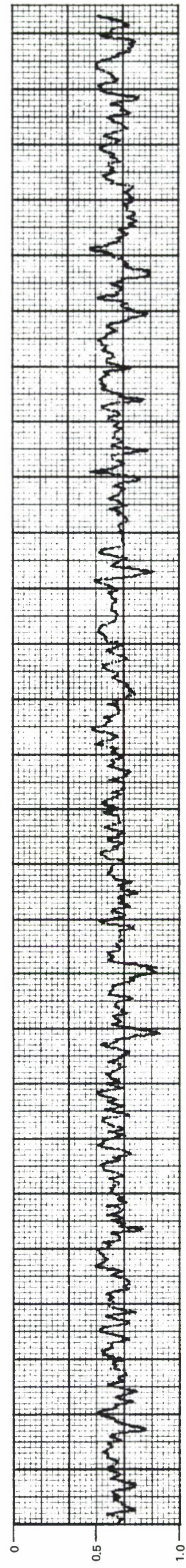
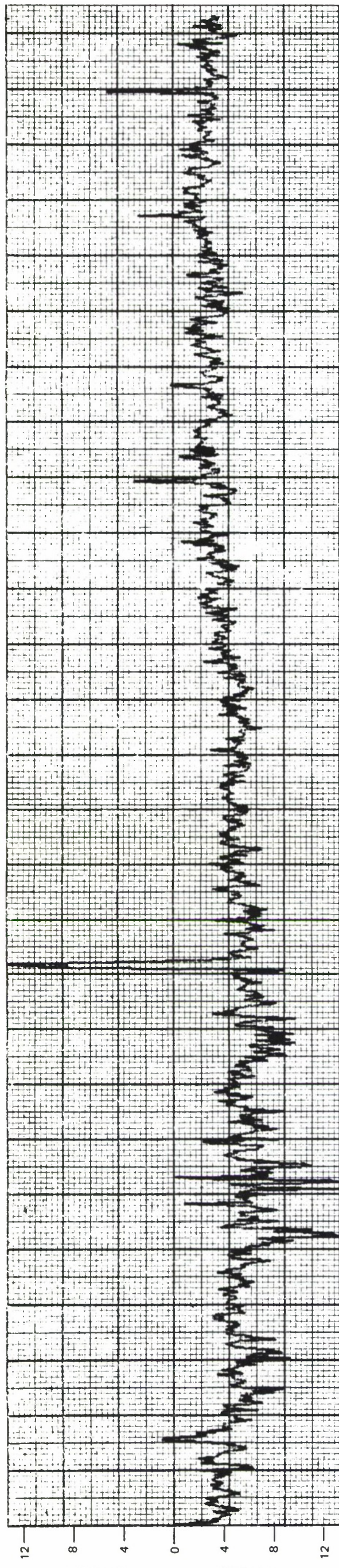


SA-2106-27

FIGURE 37 TEMPORAL DEPENDENCE OF RADIOMETER AND BAND-LIMITED WAVE-STAFF OUTPUTS FOR AUGUST 27 BEGINNING AT 1116.35

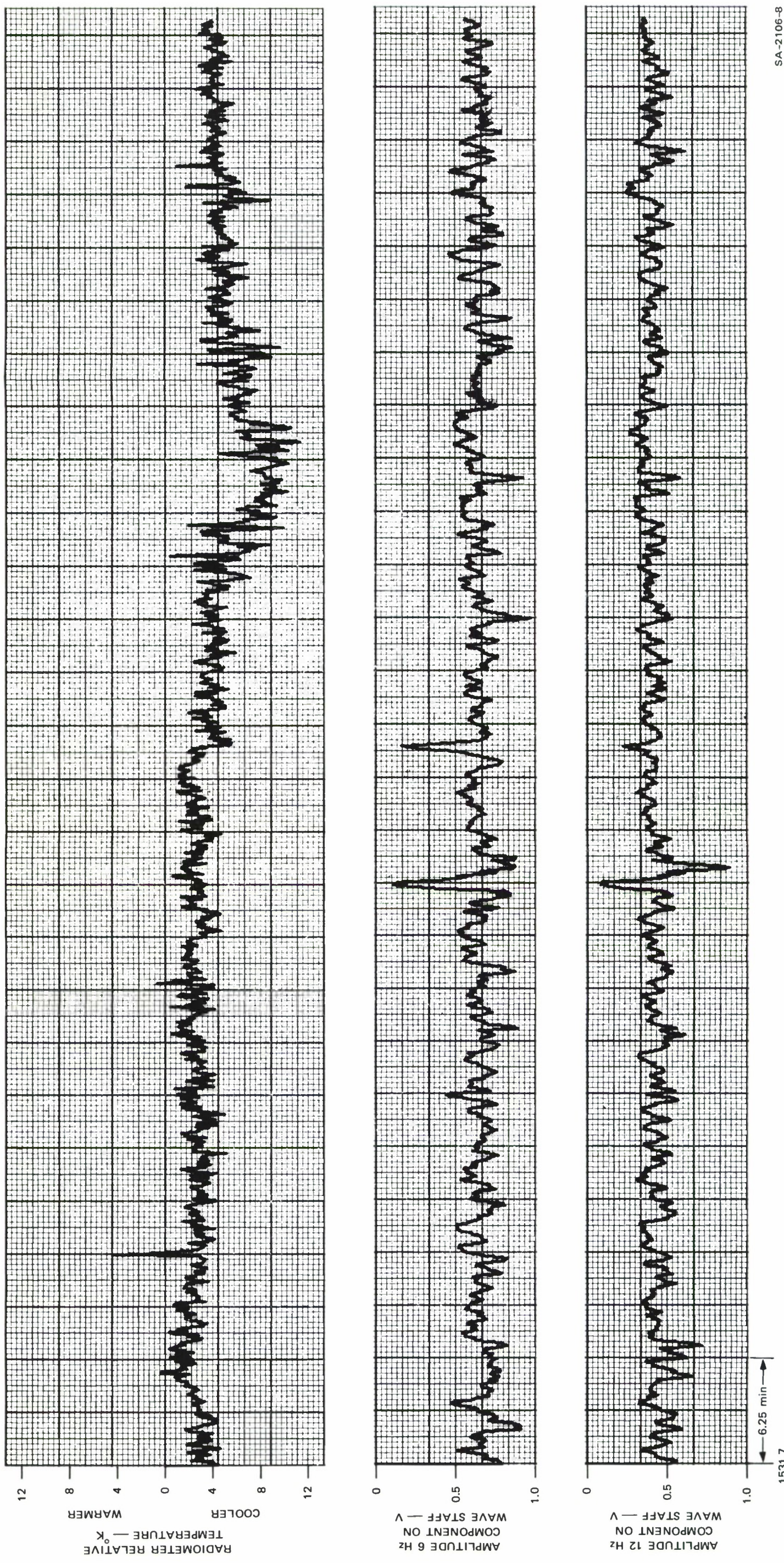


SA-2106-16  
 FIGURE 38 TEMPORAL DEPENDENCE OF  
 RADIOMETER AND BAND-  
 LIMITED WAVE-STAFF  
 OUTPUTS FOR AUGUST 27  
 BEGINNING AT 1257.75

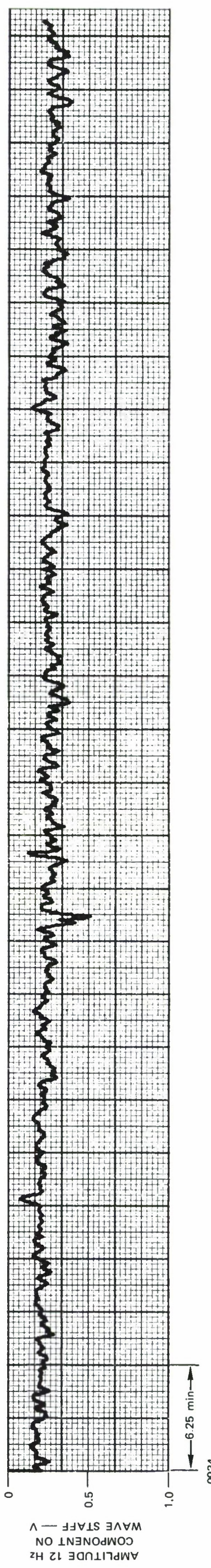
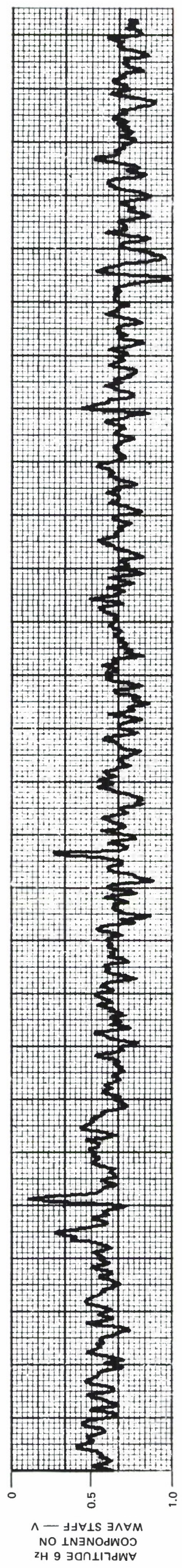
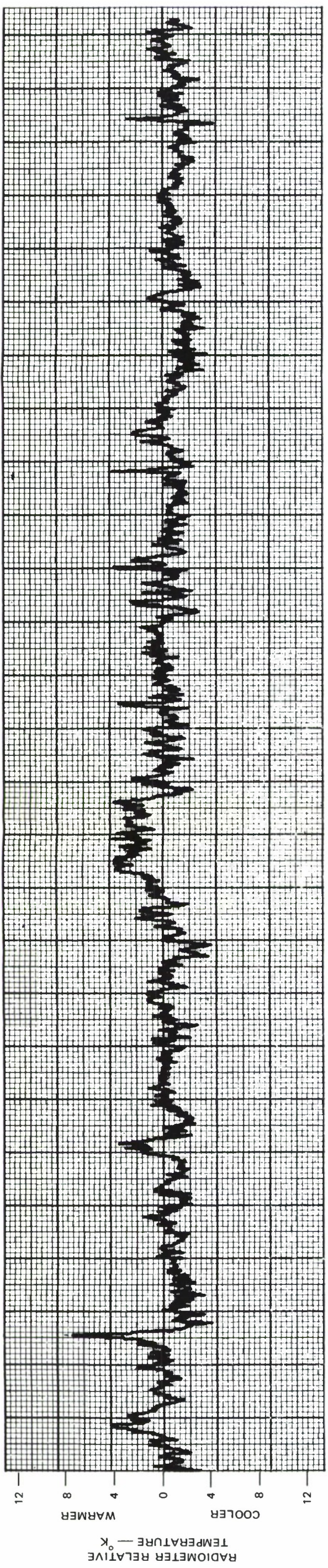


SA-2106-7

FIGURE 39 TEMPORAL DEPENDENCE OF  
RADIONOMETER AND BAND-  
LIMITED WAVE-STAFF  
OUTPUTS FOR AUGUST 27  
BEGINNING AT 1422.74

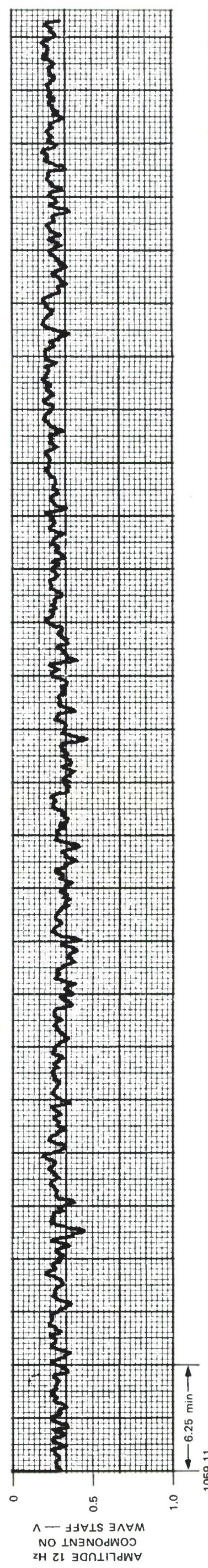
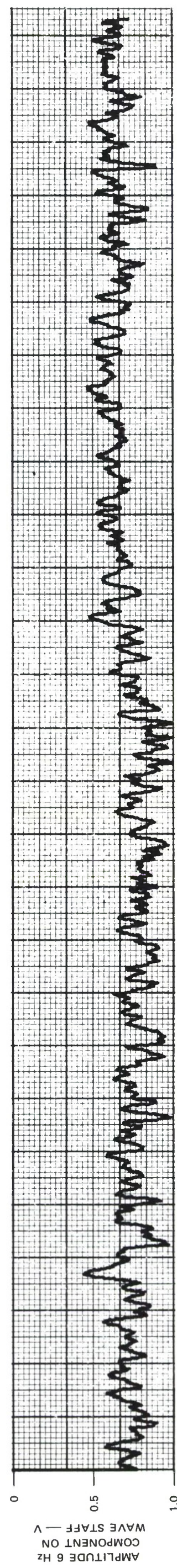
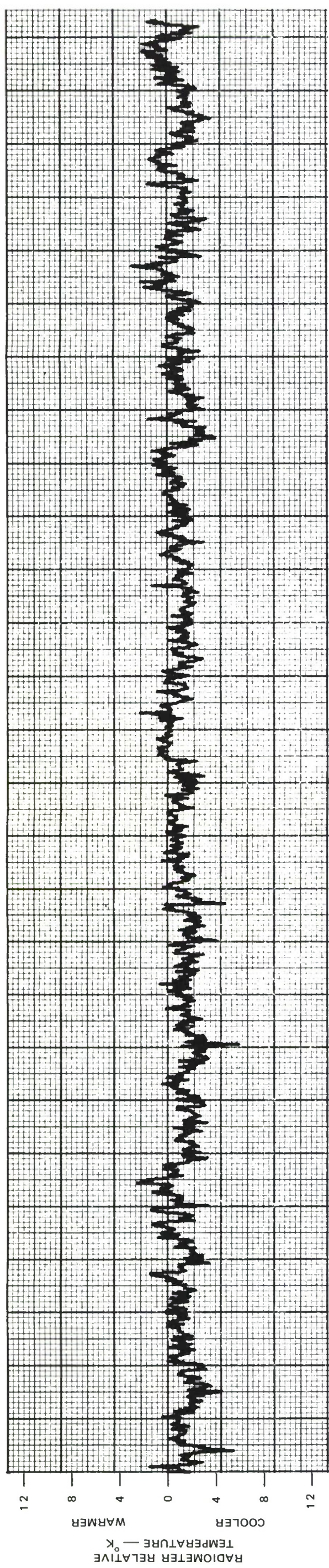


SA-2106-8  
 FIGURE 40 TEMPORAL DEPENDENCE OF  
 RADIOMETER AND BAND-  
 LIMITED WAVE-STAFF  
 OUTPUTS FOR AUGUST 27  
 BEGINNING AT 1531.7



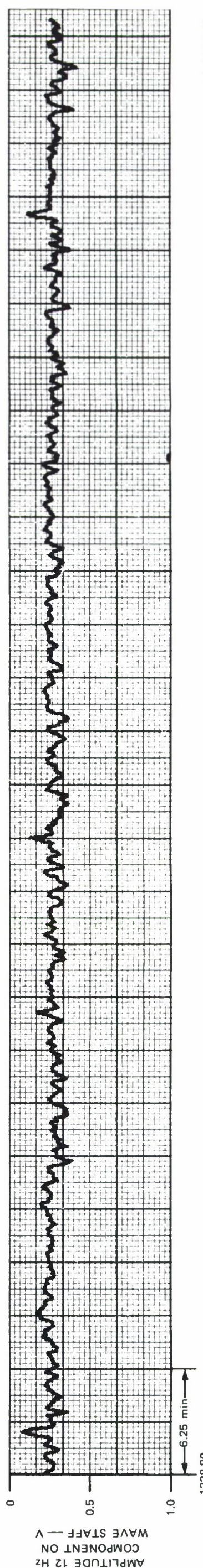
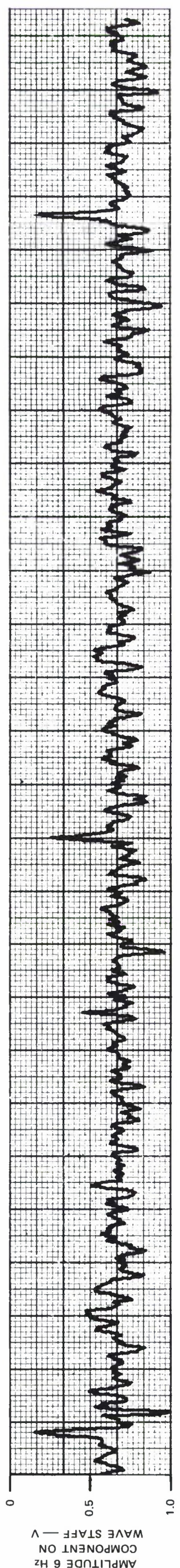
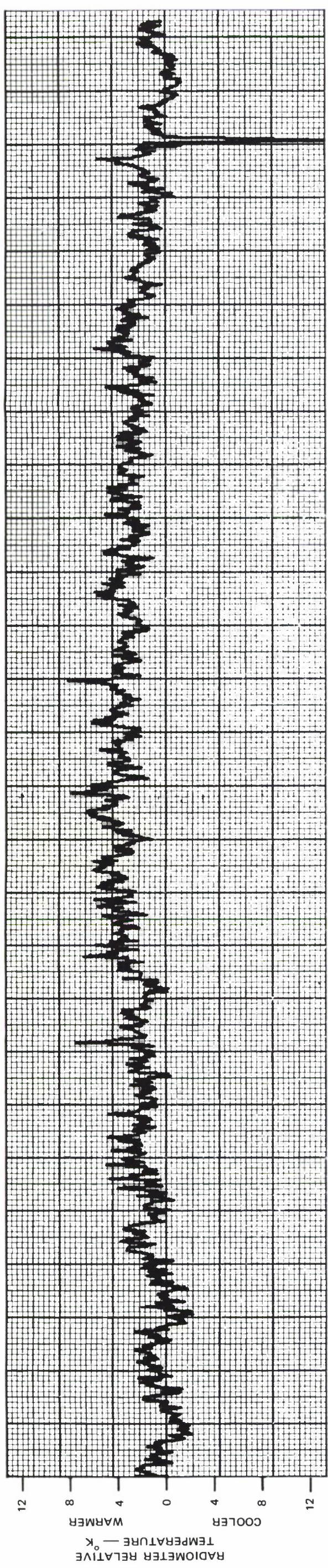
SA-2106-22

FIGURE 41 TEMPORAL DEPENDENCE OF RADIOMETER AND BAND-LIMITED WAVE-STAFF OUTPUTS FOR AUGUST 28 BEGINNING AT 0934.0



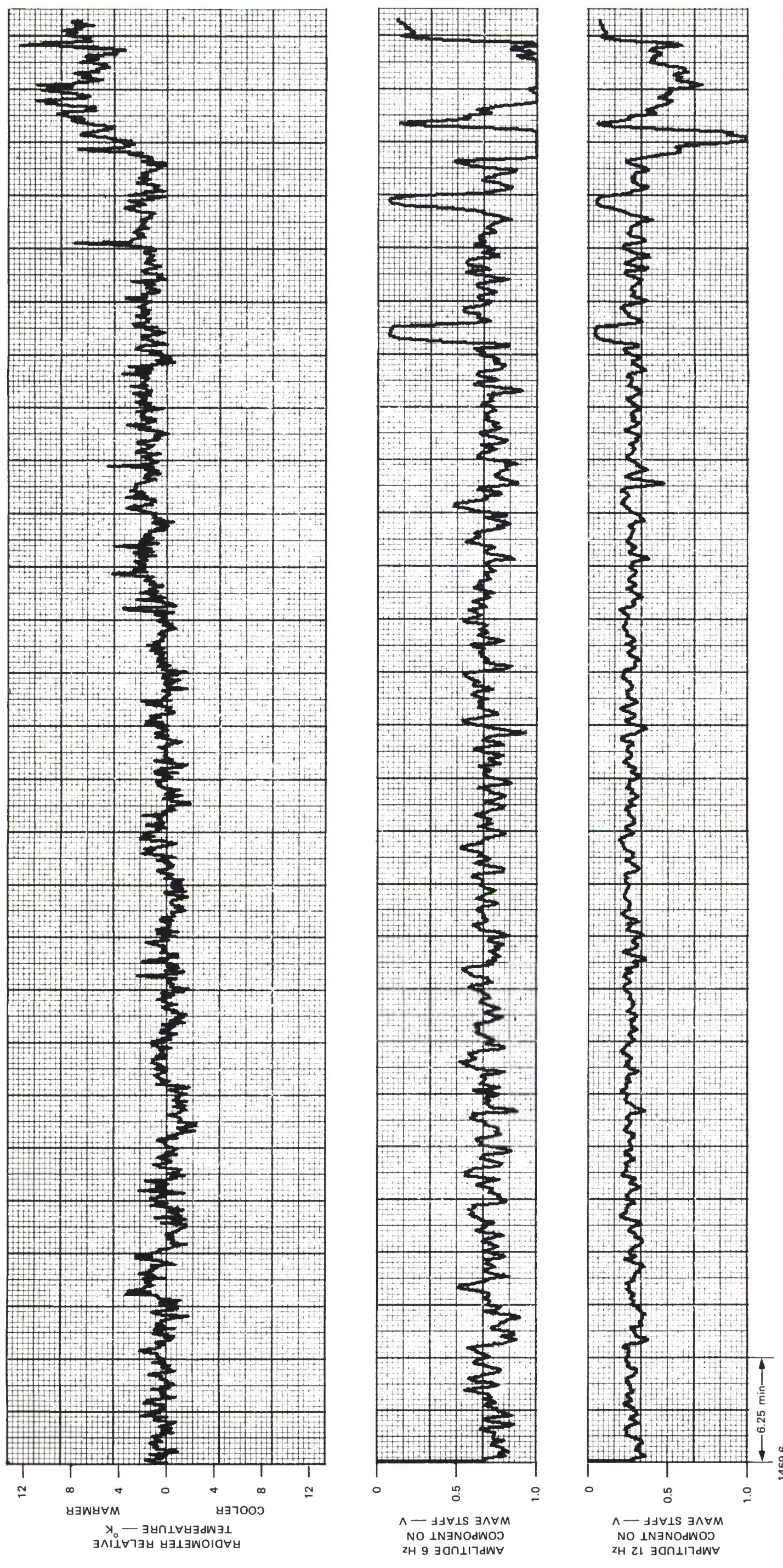
SA-2106-10

FIGURE 42  
TEMPORAL DEPENDENCE OF  
RADIOMETER AND BAND-  
LIMITED WAVE-STAFF  
OUTPUTS FOR AUGUST 28  
BEGINNING AT 1059.11

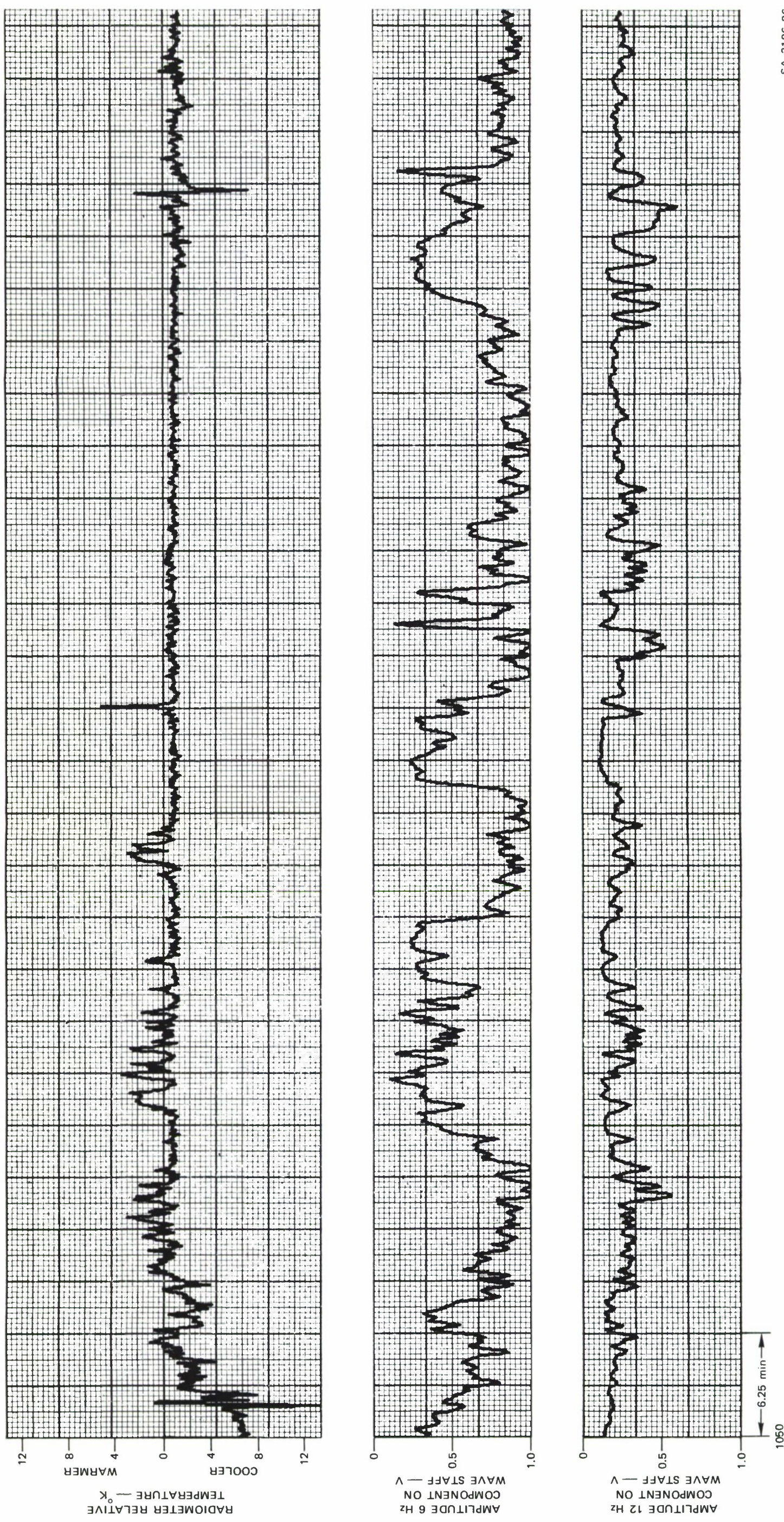


SA-2106-18

FIGURE 43 TEMPORAL DEPENDENCE OF  
RADIOMETER AND BAND-  
LIMITED WAVE-STAFF  
OUTPUTS FOR AUGUST 28  
BEGINNING AT 1328.89

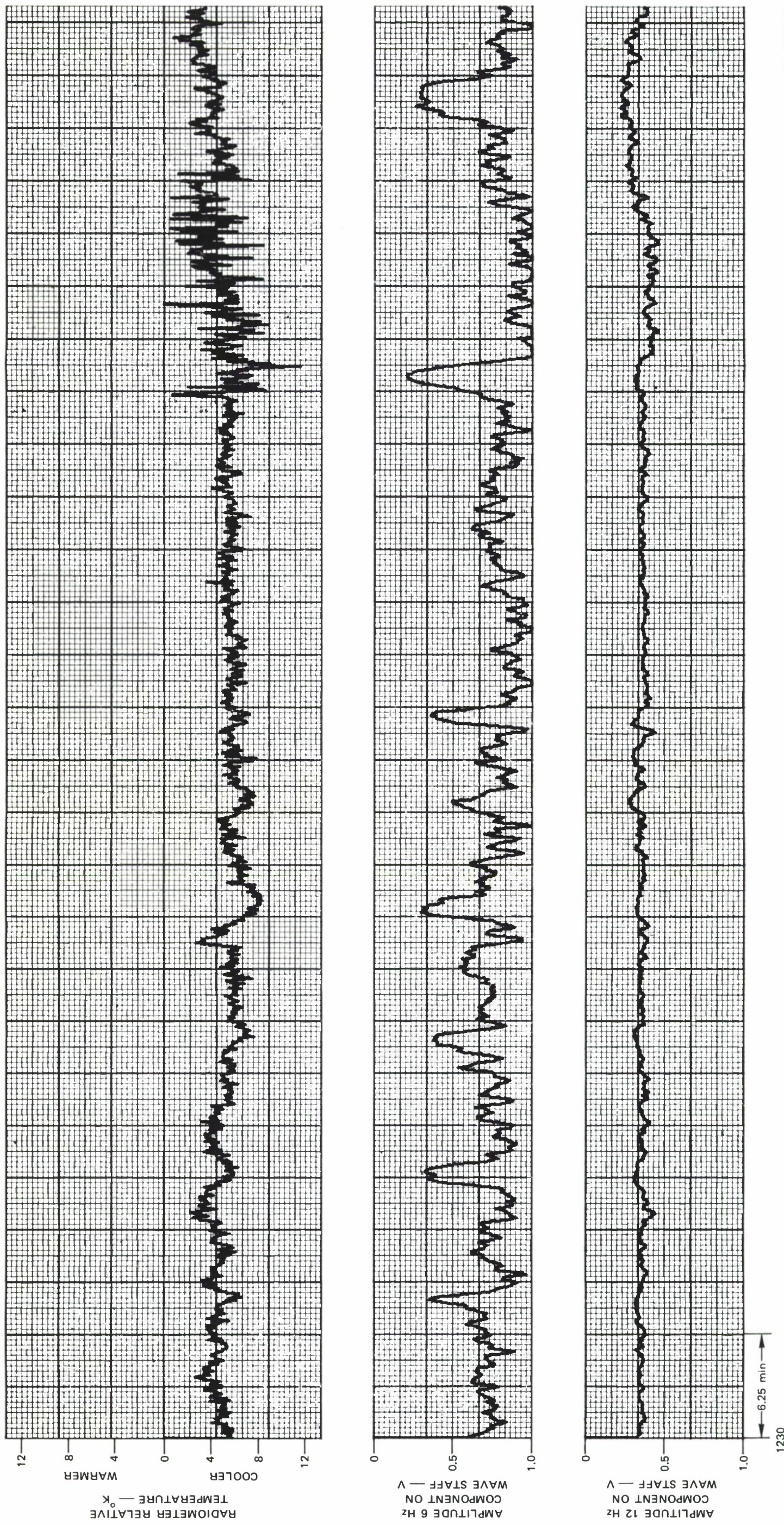


SA-2106-12  
FIGURE 44 TEMPORAL DEPENDENCE OF  
RADIONETER AND BAND-  
LIMITED WAVE-STAFF  
OUTPUTS FOR AUGUST 28  
BEGINNING AT 1459.6



SA-2106-26

FIGURE 45 TEMPORAL DEPENDENCE OF RADIOMETER AND BAND-LIMITED WAVE-STAFF OUTPUTS FOR AUGUST 30 BEGINNING AT 1050



SA-2106-25  
FIGURE 46 TEMPORAL DEPENDENCE OF  
RADIOMETER AND BAND-  
LIMITED WAVE-STAFF  
OUTPUTS FOR AUGUST 31  
BEGINNING AT 1230

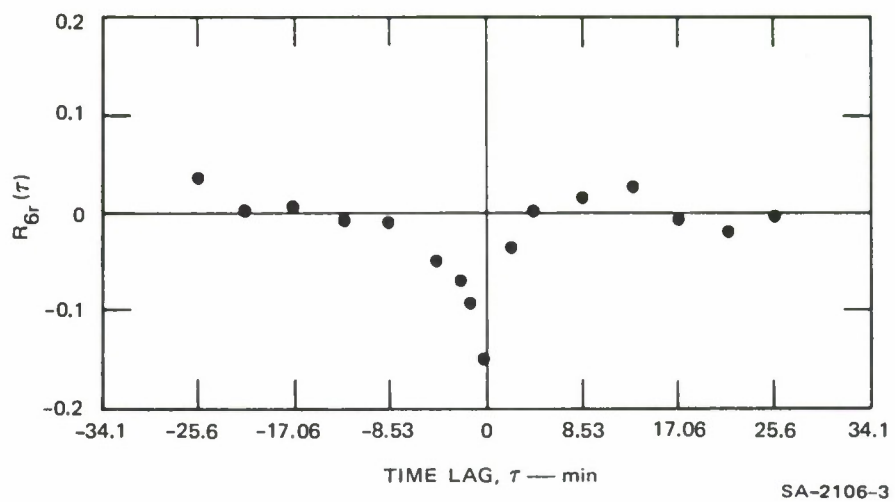


FIGURE 47 AVERAGED CROSS CORRELATION BETWEEN RADIOMETER AND AMPLITUDE OF 6-Hz COMPONENT

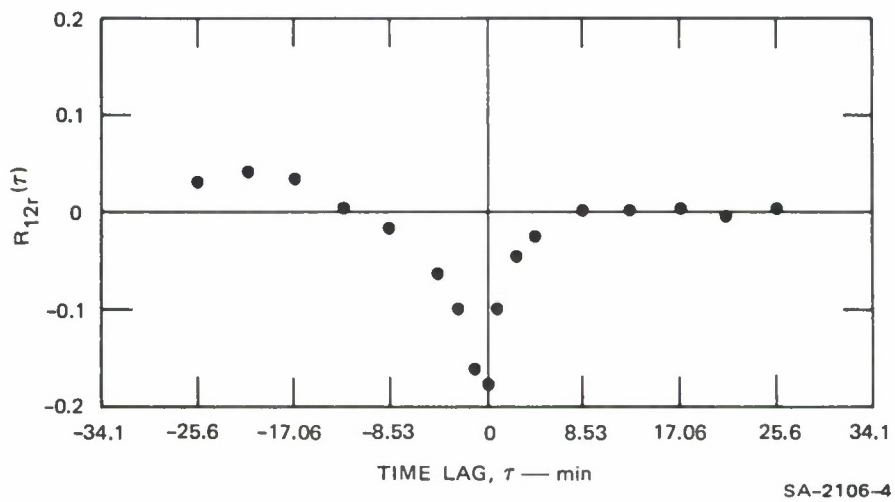


FIGURE 48 AVERAGED CROSS CORRELATION BETWEEN RADIOMETER AND AMPLITUDE OF 12-Hz COMPONENT

## V CONCLUSIONS AND RECOMMENDATIONS

Instrumentation has been designed and developed to measure the wave-height statistics, the spatial-attenuation factor of capillary waves, and the 8.9 GHz emissions of the sea surface.

The instrumentation provided by SRI has been successfully operated on the NUC oceanographic tower. The data presented in this report are only a fraction of that accumulated. The data can be profitably exploited for more information regarding the PSD of wave-height fluctuations and the emission of microwave energy by a random sea surface.

**UNCLASSIFIED**

Security Classification

## DOCUMENT CONTROL DATA - R&D

(Security classification of title, body of abstract and indexing annotation must be entered when the overall report is classified)